Upconversion-Pumped Cerium Lasers

Final Technical Report

Research Grant AFOSR 49620-98-1-0189
(Project Period 2/1/98-1/31/99)

Principal Investigator: Professor S.C. Rand

AIR FORCE OFFICE OF SCIENTIFIC RESEARCH

Program Manager
Dr. Howard Schlossberg

April 29, 1999

AFRL-SR-BL-TR-99-

0150

REPORT DOCUMENTATION PAGE

1. AGENCY USE ONLY (Leave blank)	2. REPORT DATE	3. REPORT TYPE AND DATES COVERED
	30 Apr 1999	Final 01 Feb 1998 - 31 Jan 1999

4. TITLE AND SUBTITLE
Infrared Laser Devices and Materials/Upconversion-pumped Ce Lasers

5. FUNDING NUMBERS
Grant F49620-98-1-0189

6. AUTHOR(S)
Stephen C. Rand

7. PERFORMING ORGANIZATION NAME(S) AND ADDRESS(ES)
Department of Electrical Engineering & Computer Science
University of Michigan
1301 Beal Avenue
Ann Arbor, MI 48109-2122

8. PERFORMING ORGANIZATION REPORT NUMBER
98-1467

9. SPONSORING / MONITORING AGENCY NAMES(S) AND ADDRESS(ES)
AFOSR/NE
110 Duncan Avenue Room B115
Bolling AFB, DC 20332-8050

10. SPONSORING / MONITORING AGENCY REPORT NUMBER
N/A

11. SUPLEMENTARY NOTES
The views, opinions and/or findings contained in this report are those of the author(s) and should not be construed as an official Department of the Army position, policy or decision, unless so designated by other documentation.

12a. DISTRIBUTION / AVAILABILITY STATEMENT
Approved for public release; distribution unlimited.

12b. DISTRIBUTION CODE

13. ABSTRACT (Maximum 200 words)

This project investigated the optical emission of new materials doped with Ce^{3+} for indications of practical alternatives to conventional excitation of Ce light sources. Two approaches were tried: one was based on Nd^{3+} upconversion dynamics in co-doped samples, and the other utilized electron beam pumping of Ce-doped nanopowders. Electron excitation showed exceptional promise for achieving bright emission from powders in which particle sizes averaged less than 50 nm.

14. SUBJECT TERMS
upconversion, lasers

15. NUMBER IF PAGES

16. PRICE CODE

17. SECURITY CLASSIFICATION OF REPORT	18. SECURITY CLASSIFICATION OF THIS PAGE	19. SECURITY CLASSIFICATION OF ABSTRACT	20. LIMITATION OF ABSTRACT
UNCLASSIFIED	UNCLASSIFIED	UNCLASSIFIED	UL

FINAL TECHNICAL REPORT

"Upconversion-Pumped Cerium Lasers"
(2/1/98 - 1/31/99)

I. Project Description

This program explored alternative pumping schemes for light sources emitting at near ultraviolet wavelengths of relevance to the Air Force for air-to-air communications, countermeasures and IFF applications. Two approaches were investigated in search of efficient new pathways to excite Cerium ions in dielectric host materials, Ce^{3+} being well-known for its strong emission on the inter-configurational 5d-4f transition in the neighborhood of 320 nm. The two approaches were multi-photon optical upconversion involving sensitization with secondary rare earth ions and electron beam pumping. Unusual results were obtained with both methods, but electron pumping showed unexpected promise by indicating that in powders with particle sizes less than 50 nm stimulated emission may occur.

II. Objectives

With regard to upconversion, the main objective of this project was to prepare and study novel crystals and other host solids containing trivalent Nd and Ce ions together at high concentration, in order to evaluate their promise as UV laser media. Nd was to be pumped with convenient, energy efficient near-infrared sources, and evidence sought for efficient energy transfer to the Ce^{3+} excited state. Experimentally, this called for careful assignments of observed transitions on the basis of high resolution emission spectroscopy. Another upconversion system was also studied as a testbed for the basic dynamics involved in this pumping concept in a high symmetry crystal, namely the blue-emitting compound Yb^{3+}:$CsCdBr_3$.

With regard to electron beam pumping, the original plan was to develop a method for surveying and characterizing candidate ultraviolet laser materials quickly, without the need for short wavelength pumping sources. Electron excitation and cathodoluminescence constitute a convenient way to perform ultraviolet luminescence spectroscopy, providing basic information about wavelengths and relative efficiencies of Cerium emission in a variety of hosts. This approach yielded the surprising preliminary finding that continuous-wave laser action may be possible in the nanoparticle media themselves.

III. Summary of Experimental Results

Nd was chosen as the sensitizer for Cerium in this work because of its strong absorption at diode pump wavelengths and an energy level structure capable of transferring energy efficiently to the Ce^{3+} excited state. As shown in Figure 1, multi-photon absorption pathways exist to excite Nd^{3+} to its ^2F levels, and these are nearly energy coincident with

the 5d excited state of Ce^{3+}. Hence it was of interest to record Nd upconversion emission produced by excitation at 850 nm and to see if either Nd itself or Ce could be made to emit efficiently by such means, as the result of energy transfer among the high-lying manifolds.

Upconversion emission spectra were recorded in alumina powders irradiated by a Ti:sapphire laser operating between λ=840 nm and λ=970 nm. Very narrow and very broad lines appeared together in the emission. Ordinarily such a spectrum would consist of uniformly sharp lines (typical of single crystal host materials), or uniformly broad lines

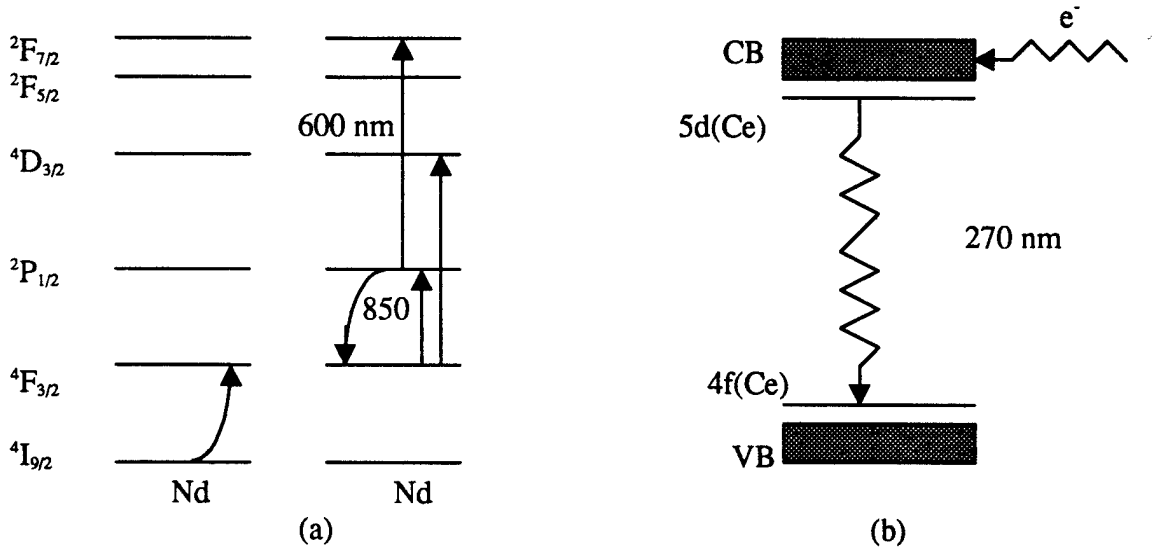

Figure 1. (a) Upconversion scheme to generate ultraviolet light from Nd nanoparticles. A "simmer" beam at 800 (or 850 nm) sustains population in the $^4F_{3/2}$ state by ground state absorption (or avalanche absorption, respectively). This population is resonantly upconverted to the $^2F_{5/2}$ state by the absorption of two red photons. (b) Electron excitation of (inter-configurational) ultraviolet emission below 300 nm from Ce^{3+} ions. Notice that the 2F levels of Nd are close to high-lying levels of Ce.

(typical of a glass host). We were surprised to find both extremes together in a single spectrum, and have insufficient data at this time to determine whether selective hybridization of particular rare earth levels is responsible for the appearance of very different linewidths for different transitions in nanoparticles or some other mechanism is at play. Preliminary results for upconversion emission from Nd,Ce:Al_2O_3 particles of 16 nm diameter containing less than 75 rare earth ions per particle are shown in Figure 2. Notice the unusual combination of very sharp and very broad spectral lines consistent with Nd transitions in this spectrum.

An unexplained aspect of the mechanism responsible for Fig.2 emission is that excitation response rises sharply at 850 nm, a wavelength corresponding to the $^4F_{3/2} \blacktriangleright {}^2P_{1/2}$ excited state transition, rather than a ground state transition, of Nd^{3+}. The response appears to be

dominated by an *excited state absorption.* Since the initial excited state ($^4F_{3/2}$) in this case lies too high in energy to be populated at room temperature, effective excitation of the system by light detuned from any ground state absorption is unexpected, but nevertheless occurs. While induced absorptions sometimes occur on excited state transitions in heavily doped bulk crystals due to "avalanche" dynamics involving many ions, such "avalanche absorption" is not expected in nanoparticles containing only a small number of impurity ions. This experimental situation limits the number of excited ions able to participate in the avalanche effect to exponentiate the induced absorption. However, the unexpected generation of upconversion emission in nanopowders clearly warrants additional study as an alternate route for the excitation of short wavelength radiation.

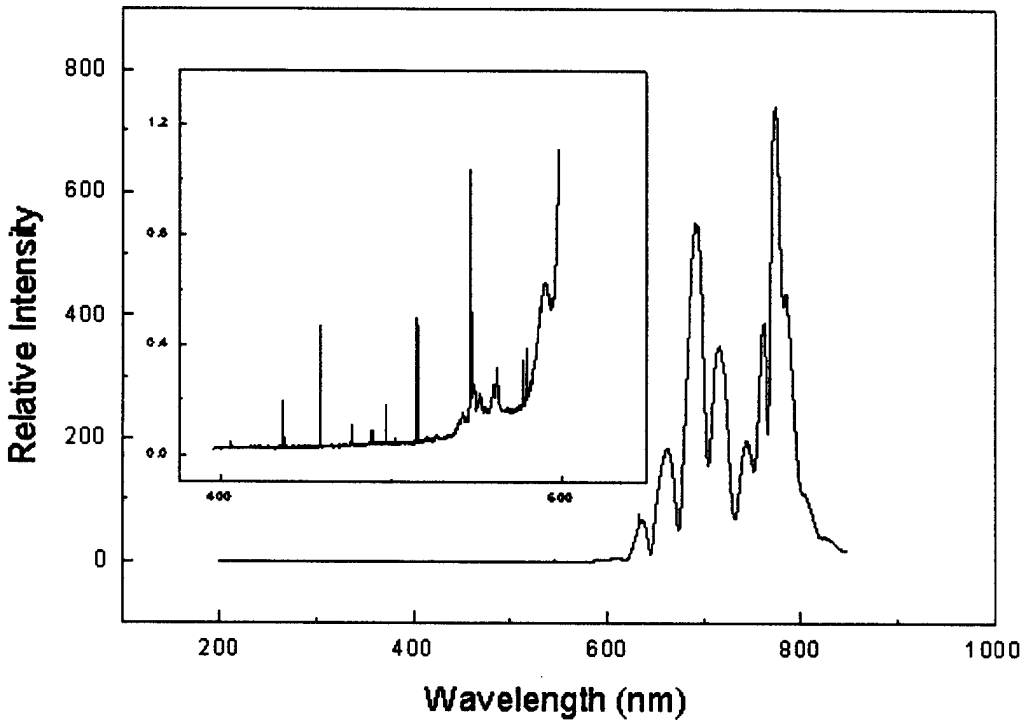

Fig. 2. Upconversion spectra of Nd,Ce:Al_2O_3 nano-particles, with the laser tuned to a wavelength of 850 nm.

Using the technique of cathodoluminescence, we were able to examine some singly- and doubly-doped oxides for strong ultraviolet and visible emission. We found that (Ce,Nd)-co-doped δ-alumina nanopowders produced by the flame spray pyrolysis technique of Prof. Laine at the University of Michigan showed no evidence of Ce emission at all when excited by an electron beam. Ultraviolet and visible spectra were dominated by instead by assignable Nd lines (Fig. 3). These spectra showed striking intensity redistribution as current was increased above a critical value however, and plots of intensity versus current exhibited a sharp break in slope at these critical or "threshold" values. When Nd

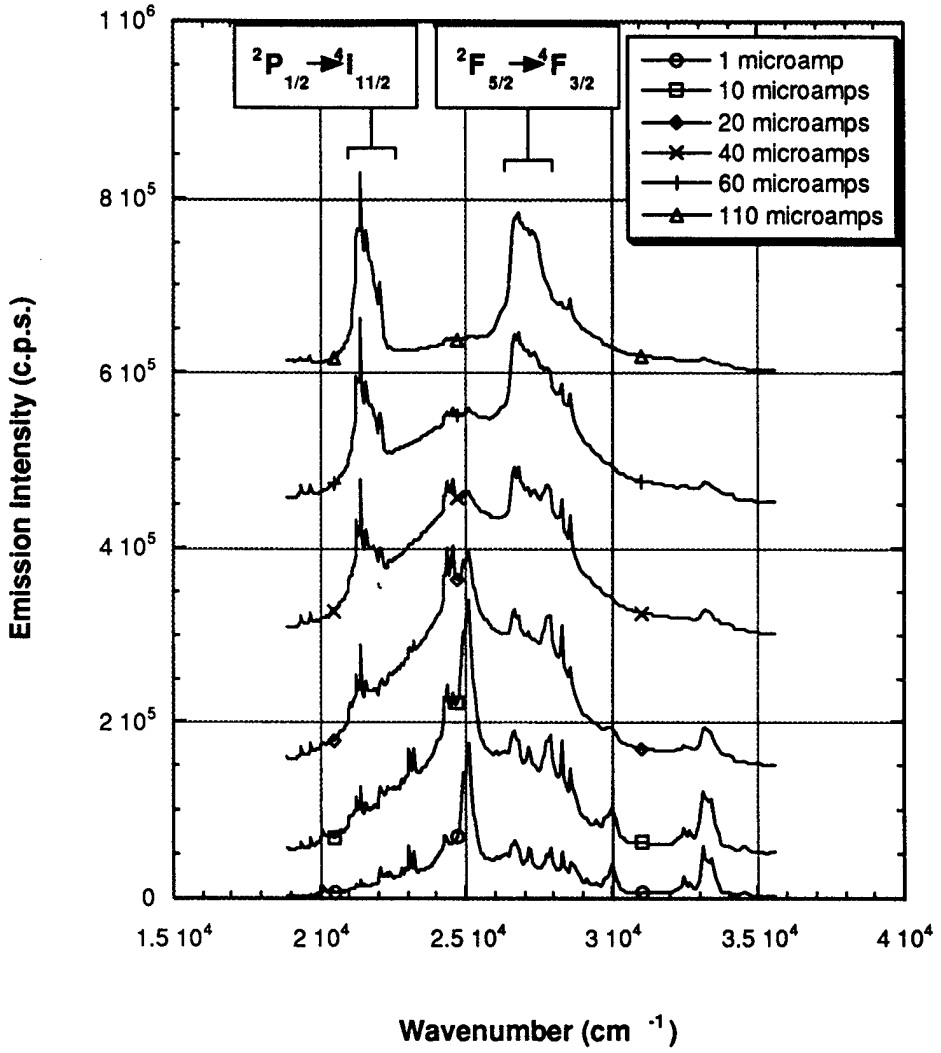

Figure 3. Nd emission excited by a 4 keV electron beam at various currents in Nd,Ce:δ-Al_2O_3 nanopowders. Spectral redistribution and quenching behavior suggest the onset of stimulated emission above 20 μA.

impurities were removed, pure Cerium-doped δ-alumina nanopowders emitted very efficiently on the 4f-5d ultraviolet line of Ce^{3+} when pumped electrically, again above an unexplained "threshold". This provided preliminary evidence of the onset of stimulated emission in our powder samples, on the emission line of interest for Air Force applications related to short wavelength radiation.

Upconversion processes in nanopowders clearly provide useful routes for excitation of ultraviolet materials with new properties. However, direct pumping with electrons seems to hold considerable promise for phosphors exhibiting stimulated emission, which is arguably more important for applications. Such media (laser phosphors) would have much higher emission rates than occur in ordinary phosphors and could be made suitable for numerous countermeasures, communication displays, targeting and IFF applications, meeting a variety of Air Force requirements.

IV. Publications

1. H. Ni, M. Hehlen. A. Lenef, J. Rai, S. Rai, Q. Shu, and S.C. Rand, "Non-radiative Dynamics of Avalanche Upconversion in Tm^{3+}:$LiYF_4$," Phys. Rev. B (pending)

2. M. P. Hehlen, A. Kuditcher and S.C. Rand, "Site-selective, intrinsically bistable luminescence in CsCd Br3: Yb^{3+}, Phys. Rev. Lett. 82, 3050(1999).

3. M. P. Hehlen, S. Luthi, A. Kuditcher and S.C. Rand, "Upconversion Mechanisms by Modulation Transform Spectroscopy in Er: $Cs_3Y_2Br_9$," Opt. Lett. (pending).

4. A. Kuditcher, M.P. Hehlen, C.M. Florea, K.M. Winick, and S.C. Rand, Intrinsically multistable luminescence and stimulated emission in Yb and Tm-doped glass", Phys. Rev. Lett. (submitted).

5. G. Williams, S.C. Rand, T. Hinklin, and R.M. Laine, "Laser Action in Strongly Scattering in Rare Earth Doped Dielectric Nanophosphors", Phys. Rev. Lett. (submitted).

6. A. Kuditcher, B. Hoover, S.C. Rand, and E. Leith, "Ultrafast, Cross-correlated imagery in the non-ballistic regime", JOSA B (in preparation).

V. Conference Proceedings

7. A. Kuditcher, B. Hoover, M.P. Hehlen, S. Rand, and E. Leith, "Time-gated harmonic imaging through scattering media," Conference on Lasers & Electro-optics (CLEO'98), San Francisco, May 5-7, 1998 (paper CWF9).

8. G.R. Williams, D. Litvinov, R. Clarke, and S.C. Rand, International Quantum Electronics Conference (IQEC'(98), San Francisco, May 5-7, 1998, paper QThI3.

9. T. Hinklin, R. Berenwall, D. Treadwell, S. Rand, and R. Laine, "Tm-doped β" -Al_2O_3 nanoparticle formation," Materials Research Society, Boston, November, 1998.

10. T. Hinklin, R. Berenwall, D. Treadwell, J. Williams, S. Rand , R. Laine, "Nano-sized luminescent oxide powders from precursors by Flame Spray Pyrolysis," Materials Research Society, Fall Meeting, Boston, November, 1998.

11. G. Williams, A. Kuditcher, S.C. Rand, T. Hinklin, R.M. Laine, "Upconversion and Cathodoluminescence of Dielectric Nanophosphors", Optical Society of America, Annual Meeting, Baltimore, Maryland, Oct. 4-9, 1998, paper TuD3.

12. S.C. Rand, A. Kuditcher, and M.P. Hehlen, "Advances in Intrinsic Optical Switching: experimental phase diagrams of critical local field effects", Optical Society of America, Annual Meeting, Baltimore, Maryland, Oct. 4-9, 1998, paper TuM3.

13. A. Kuditcher and S.C. Rand, "Intrinsic Bistability in Yb Gain Media at Room Temperature", Optical Society of America, Annual Meeting, Baltimore, Maryland, Oct. 4-9, 1998, paper FL3.

VI. Invited Presentations

14. S. Rand (plenary), Experimental Advances in Local Field Phenomena: Optical Switching and Critical Coherence" Conf. on Foundations & Applications of Quantum Optics and Quantum Mechanics, Jackson Hole, Wyoming, Aug. 3-7, 1998.

VII. Graduate Students Supported

1. Amos Kuditcher, Applied Physics Ph. D. graduate research assistant (Expected graduation July 1999).

2. Guy Williams, Applied Physics Ph. D. graduate research assistant (Expected graduation July 1999)

VII. Reprints

Site-Selective, Intrinsically Bistable Luminescence of Yb^{3+} Ion Pairs in $CsCdBr_3$

Markus P. Hehlen,* Amos Kuditcher, and Stephen C. Rand
Optical Sciences Laboratory, The University of Michigan, 1301 Beal Avenue, Ann Arbor, Michigan 48109-2122

Stefan R. Lüthi†
Department of Chemistry and Biochemistry, The University of Bern, Freiestrasse 3, 3012 Bern, Switzerland
(Received 2 December 1998)

We report the first observation of intrinsic optical bistability in $CsCdBr_3$:1% Yb^{3+} and show, using site-selective spectroscopy, that only the asymmetric, strongly coupled Yb^{3+} ion-pair minority site gives rise to hysteresis of near-infrared and cooperative up-conversion luminescence as a function of incident laser intensity below 15 K. [S0031-9007(99)08880-8]

PACS numbers: 42.65.Pc, 33.50.Hv, 42.50.Fx, 78.55.Hx

Mirrorless or intrinsic optical bistability (IOB) was first considered theoretically by Bowden and Sung [1] and extended by subsequent authors [2–5] who showed that ground state, near dipole-dipole interactions, which change the local or Lorentz-Lorenz field with respect to the incident field, could cause optical switching. The experimental observations of IOB, reported by Hehlen *et al.* in the dimer system $Cs_3Y_2Br_9$:10% Yb^{3+} [6,7] and extended to the isostructural $Cs_3Lu_2Br_9$:10% Yb^{3+} and $Cs_3Yb_2Br_9$ by Lüthi *et al.* [8], allowed for considerable refinement of the initial models. These studies identified the size of the luminescence hysteresis associated with IOB to be determined by the competition between the enhancing effect of strong, nonlinear ion-ion coupling within Yb^{3+} dimers and the degrading effect of energy migration in the Yb^{3+} sublattice. In this Letter we report for the first time the observation of IOB in a material other than the $Cs_3Yb_2Br_9$ family, demonstrating all-optical switching in the quasi-one-dimensional material $CsCdBr_3$:1% Yb^{3+} whose crystal structure suppresses energy migration at low temperatures. First, we present a statistical study of Yb^{3+} ions doped into $CsCdBr_3$ that allows for assignment of the numerous transitions observed by highly resolved laser spectroscopy to specific Yb^{3+} ion-pair sites. Second, the observation of IOB for exclusively one type of ion pair provides striking evidence that strong, nearest-neighbor ion-ion coupling is required for IOB, permitting us to estimate a maximum ion separation of ~4–5 Å for Yb^{3+} systems in which IOB can be expected to occur. Third, the temperature dependence of the luminescence hystereses is in agreement with predictions derived from earlier theory for the case of inefficient energy migration [7].

When Yb^{3+} ion pairs are excited by radiation in the near-infrared spectral region they not only emit in the near infrared from their $^2F_{5/2}$ excited-state multiplet but can also undergo cooperative up-conversion yielding emission in the blue-green spectral region from the doubly excited $[^2F_{5/2}, {}^2F_{5/2}]$ pair state which results from ion-ion coupling [9–11]. Since the coupling strength between Yb^{3+} ions is a strong function of the ion separation, cooperative up-conversion is highly favored in pair-forming materials [10,12]. Likewise, IOB is expected to be favored in such materials [6,7]. Therefore we chose to investigate $CsCdBr_3$, a host that crystallizes in the D_{6h}^4 space group with lattice constants $a = 7.675$ Å and $c = 6.722$ Å and that consists of linear chains of face-sharing $[CdBr_6]^{4-}$ units, with the chains arranged along the **c** axis and the Cs^+ ions occupying high-symmetry sites between the chains [13]. A key feature of $CsCdBr_3$ is the formation of isolated, charge-compensated ion-pair centers when tripositive rare-earth ions such as Yb^{3+} are incorporated onto the Cd^{2+} lattice position. The main impurity site is then a symmetric in-chain Yb^{3+}-(Cd^{2+} vacancy)-Yb^{3+} ion pair (Yb-V-Yb) [14,15]. The two most abundant minority sites are the asymmetric in-chain Yb^{3+}-Yb^{3+}-(Cd^{2+} vacancy) ion pair (Yb-Yb-V) [16–20] and the Yb^{3+}-(Cs^+ vacancy) site [16,21]. The requirement for charge compensation, in contrast to most other crystal systems, provides for a high yield of Yb^{3+} ion pairs relative to Yb^{3+} single-ion sites, and, as a consequence, a sizable Yb^{3+} ion-pair concentration can be obtained even at low Yb^{3+} ion densities for which undesired energy migration through the Yb^{3+} sublattice is still relatively inefficient.

Coupling between Yb^{3+} ions mainly occurs within the symmetric Yb-V-Yb ($R \approx 6.7$ Å) and asymmetric Yb-Yb-V ($R \approx 3.4$ Å) ion pairs since its strength decreases rapidly with increasing ion separation R. Both forced dipole-dipole (dd) and dipole-quadrupole (dq) interactions are significant for short-range intrapair coupling with the former dominating for $R > 8$ Å [11]. In addition, there are interpair interactions the relative importance of which depends on the Yb^{3+} ion-pair density. Earlier studies of $CsCdBr_3$:Pr^{3+} found the asymmetric ion pair to be thermodynamically unstable and to transform into the stable symmetric ion pair at $T > 350$ °C and even at room temperature over extended periods [22]. Therefore, the fraction, F, of asymmetric ion pairs depends on the thermal history of the sample. In order to quantify relative intra- and interpair interactions in the $CsCdBr_3$:1% Yb^{3+} crystal studied here a numerical study of the probability distribution of R with F as a parameter was carried out. A computer model defined the Cd^{2+} sublattice that consisted

of $\sim 5 \times 10^5$ $CsCdBr_3$ unit cells and in which 1% of the $\sim 10^6$ Cd^{2+} ions was randomly replaced by Yb^{3+} ions that were forced to form either the Yb-V-Yb or the Yb-Yb-V ion pair in a given ratio F; other types of defect sites and lattice distortions were not considered. For each Yb^{3+} ion the distance to all other Yb^{3+} ions was subsequently calculated and recorded in a histogram (Fig. 1, left), yielding a >95% statistical confidence level. The probability distribution for $R < 20$ Å is dominated, as expected, by the most abundant symmetric Yb-V-Yb intrapair ion distance of 6.7 Å, and the Yb-Yb-V intrapair distance at 3.4 Å becomes increasingly important as the asymmetric ion-pair density increases with F. In addition, there are four interpair distances below 12 Å that are significant at this 5.8×10^{19} Yb^{3+} per cm^3 ion density. These are interchain distances between Yb^{3+} ions offset by 0, $\frac{1}{2}$, and 1 lattice constant (c) at 7.7, 8.4, and 10.2 Å, respectively, and the closest interpair in-chain distance at 10.1 Å. Since doping $CsCdBr_3$ with Yb^{3+} ions creates lattice defects one expects the individual Yb^{3+} resonance frequencies to depend (i) on the respective intrapair distance and (ii) on ion pairs in the immediate surroundings. Assuming the Yb^{3+} transition cross sections to be independent on ion-ion coupling, the distance distribution weighted by the distance dependence of ion interaction (dd and dq coupling [11]) is proportional to the intensity of cooperative emission from Yb^{3+} ion pairs (Fig. 1, right). From this statistical ion-distribution model one concludes that (i) the relative up-conversion intensity from asymmetric vs symmetric ion pairs is a measure for F (with the spectrum being dominated by asymmetric and symmetric ion pairs for $F > 0.01$ and $F \leq 0.01$, respectively) and that (ii) the various intra- and interpair interactions result in a multitude of Yb^{3+} resonance frequencies and thus more than one transition in the spectrum.

Figure 2, top, shows unpolarized luminescence excitation spectra of the $^2F_{7/2}(0) \rightarrow {}^2F_{5/2}(2')$ transition in a $CsCdBr_3$:1% Yb^{3+} single crystal at 7 K recorded by frequency scanning a single-mode (TEM_{00}), actively power-stabilized Ti:sapphire laser and simultaneously monitoring both the near-infrared (NIR) and the cooperative visible (VIS) luminescence intensity. The strong trigonal distortion of the sixfold bromide coordination of Yb^{3+} in $CsCdBr_3$ lifts the J degeneracy and splits the $^2F_{7/2}$ and $^2F_{5/2}$ ground and excited-state multiplets in four and three Kramers doublets, respectively. The $^2F_{7/2}(0) \rightarrow {}^2F_{5/2}(2')$ crystal-field transition used for excitation around 10 600 cm^{-1} in this study therefore is, in the absence of any Yb^{3+} ion interactions, expected to consist of a single line. The many lines observed in the excitation spectra in this narrow frequency region are direct evidence for the existence of several structurally different charge-compensated Yb^{3+} ion pairs, each potentially distorted by additional interpair interactions and thus each with an individual $^2F_{7/2}(0) \rightarrow {}^2F_{5/2}(2')$ resonance frequency. The strongest line centered at 10 601 cm^{-1} contains ~60% of the total intensity, a value that is likely underestimated given the presence of a slight absorption rate saturation at the 500 W/cm^2 excitation density used here. We assign this line to the undistorted Yb-V-Yb symmetric ion pair on the basis of its high abundance [16]. A variety of second-order distortions of that site, such as the many interpair interactions described in the numerical analysis above, may shift the resonance frequency of each Yb^{3+} ion of a pair, and consequently a number of distinct transitions in this $^2F_{7/2}(0) \rightarrow {}^2F_{5/2}(2')$ frequency range are

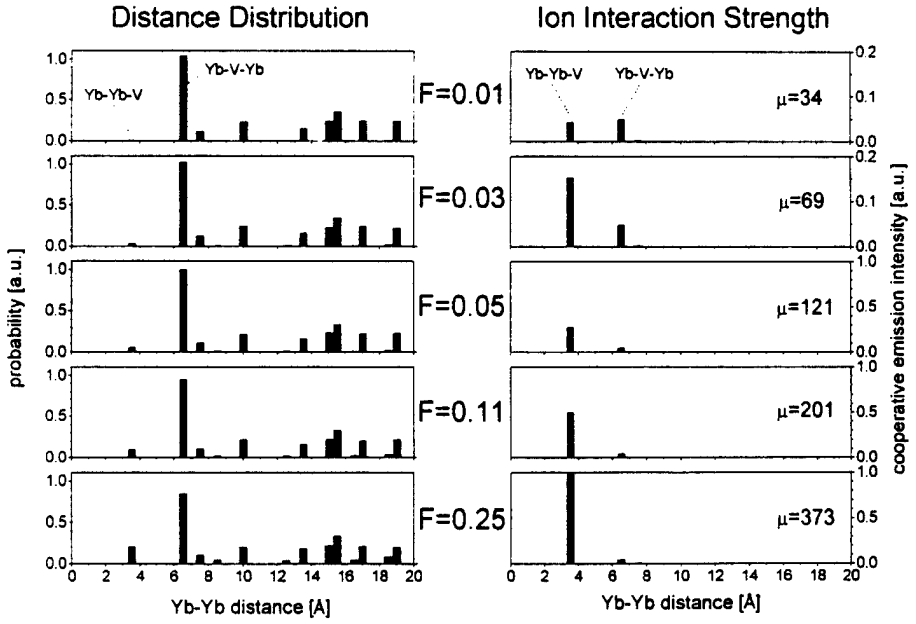

FIG. 1. Statistical ion-distribution analysis of $CsCdBr_3$:1% Yb^{3+} for various fractions $F = n_a/(n_a + n_s)$, where n_a and n_s are asymmetric (Yb-Yb-V) and symmetric (Yb-V-Yb) ion-pair densities, respectively. Normalized probability distributions of Yb^{3+}-Yb^{3+} ion distances (left) are weighted by the distance dependence of the ion interaction (dd and dq [11]) strength (right). μ denotes the ratio of intra- and interpair energy-transfer rate constants derived from the calculation.

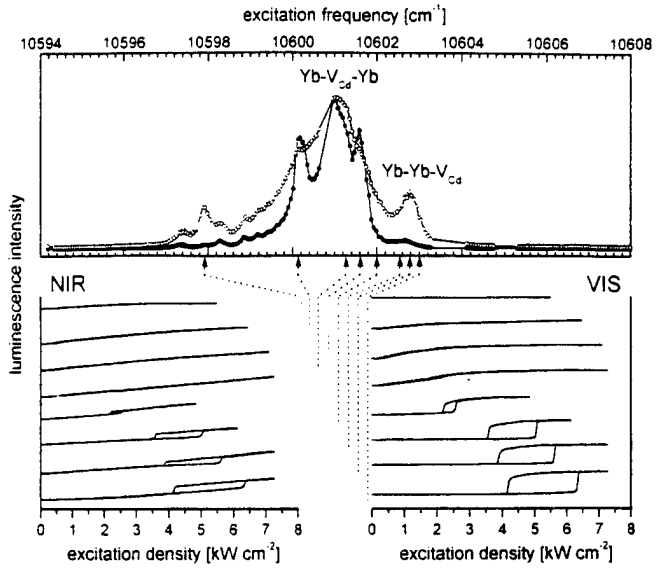

FIG. 2. Site-selective IOB in $CsCdBr_3$:1% Yb^{3+} at 7 K. Top: unpolarized excitation spectra for NIR (open circles) and VIS (solid circles) Yb^{3+} emission. Bottom: NIR and VIS luminescence hystereses as a function of excitation density for various excitation frequencies.

observed. The resonance frequency of the undistorted asymmetric Yb-Yb-V ion pair is expected to be larger than that of the symmetric Yb-V-Yb pair, since the close 3.4 Å intrapair separation of the two Yb^{3+} ions induces a large axial field which increases the $^2F_{5/2}$ crystal-field splitting. We therefore assign the highest-energy transition at 10 602.8 cm^{-1} to the undistorted Yb-Yb-V asymmetric ion pair. With these assignments in Fig. 2, the ratio of up-conversion intensities of asymmetric and symmetric ion pairs is found to be <1, and, based on the statistical ion-distribution model, we find that $F < 0.01$. The relatively small number of asymmetric ion pairs is consistent with both earlier studies and the Bridgman crystal growth conditions. The crystal studied here was grown by lowering an ampoule at a slow speed of 0.6 mm/h from 415 °C through a temperature gradient of 20 °C per cm during two weeks, a process that not only led to high-quality crystals but also provided for *in situ* annealing at elevated temperatures, thereby transforming many thermodynamically unstable asymmetric ion pairs to stable symmetric ion pairs.

The Yb^{3+} site assignments derived above are consistent with the wavelength dependence of IOB in $CsCdBr_3$:Yb^{3+}. When the laser intensity is varied at a fixed excitation frequency, hysteresis in the near-infrared luminescence (Fig. 2, bottom left) and in the visible cooperative up-conversion luminescence (Fig. 2, bottom right) is observed exclusively for excitation of the 0.6 cm^{-1} (FWHM) wide line centered at 10 602.8 cm^{-1} that was assigned to the asymmetric Yb-Yb-V minority site. For this site, intrapair coupling between the Yb^{3+} ions is inferred to be the strongest and the cooperative up-conversion rate constant α the largest, in view of the fact that the corresponding ion-ion distance of 3.4 Å in the nearest-neighbor face-sharing $[Yb_2Br_9]$ ion-pair coordination is the smallest. A reduction of α by a factor of ~ 100 (dd and dq coupling) is expected for the symmetric Yb-V-Yb ion-pair main site relative to the asymmetric Yb-Yb-V site: the symmetric ion pair showed no IOB (Fig. 2). We conclude that at Yb^{3+} ion separations below 4–5 Å, α exceeds a critical threshold value for which IOB becomes active. This restricts coordination geometries to nearest-neighbor face sharing, possibly nearest-neighbor edge sharing, Yb^{3+} ion pairs in IOB compounds. This conclusion was not possible in earlier studies of $Cs_3Y_2Br_9$:10% Yb^{3+} [6–8] in which Yb^{3+} ions statistically substitute for Y^{3+} without preferential pair formation in a distribution of separations exceeding 5.8 Å, besides the 3.8 Å of the crystallographic $[Yb_2Br_9]^{3-}$ dimer unit. Our findings here suggest that also in $Cs_3Y_2Br_9$:Yb^{3+}, IOB is due only to the nearest-neighbor face-sharing $[Yb_2Br_9]^{3-}$ coordination.

Although both $Cs_3Lu_2Br_9$:10% Yb^{3+} and $CsCdBr_3$:1% Yb^{3+} share the structurally very similar $[Yb_2Br_9]^{3-}$ coordination as the ion pair responsible for IOB, some of the optical switching properties of the two compounds are fundamentally different. First, although IOB gradually disappears in both compounds with increasing temperature, the hysteresis step height remains almost constant in $CsCdBr_3$:1% Yb^{3+} whereas in $Cs_3Lu_2Br_9$:10% Yb^{3+} it decreases monotonically in concert with the area of IOB hysteresis loops (Fig. 3). Second, the switching polarity of both the NIR and VIS emissions is the same (Fig. 2), in contrast to the opposite switching polarity that was observed in $Cs_3Y_2Br_9$:10% Yb^{3+} [7]. Earlier theoretical work showed [6,7] that the key features of IOB in Yb^{3+}-doped compounds can be qualitatively explained by the steady-state solution of the density matrix of coupled two-level systems driven by a radiation field. It was found that an increasing dephasing rate constant decreases the hysteresis width, step height, and critical incident intensities. Although various mechanisms such as energy migration, electron-phonon interaction, and cooperative interaction can contribute to dephasing, it is the rate constant, β, for energy migration through the Yb^{3+} sublattice that is profoundly different in the two materials. In $Cs_3Lu_2Br_9$:10% Yb^{3+}, energy migration between the $[Yb_2Br_9]^{3-}$ dimer units is fast due to the high Yb^{3+} single-ion density of $\sim 3.9 \times 10^{20}$ cm^{-3} and the correspondingly high probability for a Yb^{3+} neighbor within the critical energy-transfer radius. Long-range energy migration is efficient and thus the dephasing rate constant is large and expected to increase with increasing temperature. In $CsCdBr_3$:1% Yb^{3+}, on the other hand, the majority of Yb^{3+} ions form ion pairs yielding an ion-pair density of $\sim 2.9 \times 10^{19}$ cm^{-3} and thus a large interpair separation on average. From the $F < 0.01$ case relevant for the crystal studied here we estimate interpair energy transfer to be up to ~ 34 times less likely than intrapair energy transfer (indicated in Fig. 1, right, by the ratio μ), i.e., $\beta < \alpha$. Thus, long-range energy migration is strongly suppressed in $CsCdBr_3$:1% Yb^{3+}, and dephasing from this source is expected to be small and fairly independent of temperature.

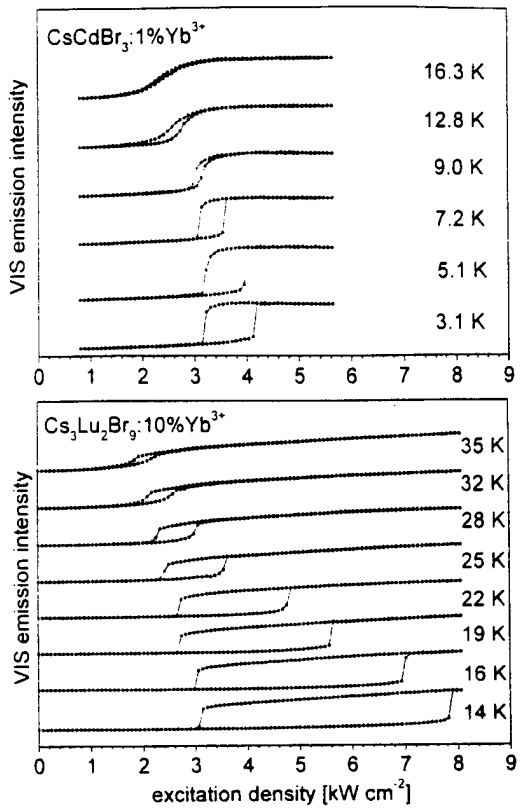

FIG. 3. Temperature dependence of IOB in $CsCdBr_3$:1% Yb^{3+} (top) and $Cs_3Lu_2Br_9$:10% Yb^{3+} (bottom) recorded under identical conditions. The hystereses of visible cooperative Yb^{3+} emission intensity as a function of excitation density were excited in the near infrared at 10 602.8 and 10 592.0 cm^{-1}, respectively.

This result explains the relative insensitivity of the hysteresis step height in $CsCdBr_3$:1% Yb^{3+} as compared to $Cs_3Lu_2Br_9$:10% Yb^{3+} (Fig. 3). Similarly, the migrational differences between the two materials account for the reversals of the switching polarity in the NIR and VIS hystereses. In $CsCdBr_3$:1% Yb^{3+}, the ion pairs responsible for IOB are isolated, and when the excited-state population increases upon switching both the NIR and VIS emissions luminescence originating from this state will increase in intensity; the switching polarity of the VIS and NIR emissions is the same. However, if migration is fast as in $Cs_3Lu_2Br_9$:10% Yb^{3+}, the large reservoir of Yb^{3+} single ions determines the NIR emission intensity. The loss of population from this group that occurs upon switching due to an increase of VIS emission from paired impurities causes the switching polarity to be opposite.

In summary, we have extended IOB to a new material, $CsCdBr_3$:1% Yb^{3+}, and have concluded from site-selective optical switching experiments and a statistical study of the Yb^{3+} ion distribution that ion separations below ~4–5 Å are required for IOB to become active in Yb^{3+} systems. It is concluded that crystal-growth conditions favoring asymmetric ion pairs in $CsCdBr_3$:1% Yb^{3+} would strongly enhance the intensities of the switching transitions. A comparison of $CsCdBr_3$:1% Yb^{3+} and $Cs_3Lu_2Br_9$:10% Yb^{3+} has revealed the key role of energy migration in determining both the temperature dependence and the switching polarity of IOB. These results provide guidelines for expanding the materials basis in the search for high-temperature IOB systems.

M. P. H. thanks the Swiss National Science Foundation for financial support through an Advanced Researcher Fellowship. We thank H. U. Güdel, K. Krämer, and N. Furer, University of Bern, for preparing the crystals and providing the sample cells. This work was partially supported by the Air Force Office of Scientific Research Grant No. F49620-98-1-0189.

*Current address: Gemfire Corporation, 2471 E. Bayshore Road, Palo Alto, CA 94303.
Email address: M.Hehlen@gemfirecorp.com
†Current address: Department of Chemistry, The University of Queensland, Brisbane, Qld 4072, Australia.

[1] C. M. Bowden and C. C. Sung, Phys. Rev. A **19**, 2392 (1979).
[2] F. A. Hopf, C. M. Bowden, and W. Louisell, Phys. Rev. A **29**, 2591 (1984).
[3] F. A. Hopf and C. M. Bowden, Phys. Rev. A **32**, 268 (1985).
[4] Y. Ben-Aryeh, C. M. Bowden, and J. C. Englund, Phys. Rev. A **34**, 3917 (1986).
[5] M. E. Crenshaw, M. Scalora, and C. M. Bowden, Phys. Rev. Lett. **68**, 911 (1992).
[6] M. P. Hehlen, H. U. Güdel, Q. Shu, J. Rai, S. Rai, and S. C. Rand, Phys. Rev. Lett. **73**, 1103 (1994).
[7] M. P. Hehlen, H. U. Güdel, Q. Shu, and S. C. Rand, J. Chem. Phys. **104**, 1232 (1996).
[8] S. R. Lüthi, M. P. Hehlen, T. Riedener, and H. U. Güdel, J. Lumin. **76&77**, 447 (1998).
[9] E. Nakazawa and S. Shionoya, Phys. Rev. Lett. **25**, 1710 (1970).
[10] M. P. Hehlen and H. U. Güdel, J. Chem. Phys. **98**, 1768 (1993).
[11] Ph. Goldner, F. Pellé, D. Meichenin, and F. Auzel, J. Lumin. **71**, 137 (1997).
[12] F. Auzel, D. Meichenin, F. Pellé, and Ph. Goldner, Opt. Mater. **4**, 35 (1994).
[13] D. Visser, G. C. Verschoor, and D. J. W. Ijdo, Acta Crystallogr. Sect. B **36**, 28 (1980).
[14] G. L. McPherson and L. M. Henling, Phys. Rev. B **16**, 1889 (1977).
[15] L. M. Henling and G. L. McPherson, Phys. Rev. B **16**, 4756 (1977).
[16] J. Neukum, N. Bodenschatz, and J. Heber, Phys. Rev. B **50**, 3536 (1994).
[17] C. Barthou and R. B. Barthem, J. Lumin. **46**, 9 (1990).
[18] N. J. Cockroft, G. D. Jones, and D. C. Nguyen, Phys. Rev. B **45**, 5187 (1992).
[19] Ph. Goldner and F. Pellé, J. Lumin. **55**, 197 (1993).
[20] M. Mujaji, G. D. Jones, and R. W. G. Syme, Phys. Rev. B **48**, 710 (1993).
[21] G. L. McPherson and K. O. Devaney, J. Phys. C **13**, 1735 (1980).
[22] J. Heber, U. Schäfer, J. Neukum, and N. Bodenschatz, Acta Phys. Pol. A **84**, 889 (1993).

Intrinsically multistable luminescence and stimulated emission in Yb and Tm–doped glass

A. Kuditcher*, M. P. Hehlen†, C. M. Florea, K. W. Winick, and S. C. Rand*

Department of Electrical Engineering and Computer Science,

1301 Beal Avenue, University of Michigan, Ann Arbor, MI 48109-2122

(November 20, 1998)

Abstract

Intrinsic bistability, multistability and hysteresis have been observed in the photoluminescence of bulk glass doped with Yb^{3+} and Tm^{3+} impurities at room temperature. Hysteretic switching of laser output also occurs near threshold in channel waveguides in this material. Local field effects are shown to present new, fundamental design limitations for compact optical amplifiers and oscillators.

42.65.Pc

Typeset using REVTEX

*Also at: Division of Applied Physics, University of Michigan

†Present address: Gemfire Corporation, 2471 E. Bayshore Road, Palo Alto, CA, 94303

Nearly a century ago, Lorentz developed an elegant theory for the optical polarization of matter [1] which introduced the concept of local fields. He calculated a correction for fields incident on a solid which yielded the internal field value using a simple, approximate procedure applicable to many materials. This theory was reformulated and extended for specific crystal structures subsequently by a number of authors [2,3]. With the advent of nonlinear optics [4] and the discovery of phenomena such as surface-enhanced Raman scattering [5], local field corrections were gradually recognized as being important for quantitative explanations of some optical interactions with matter because of the multiplicative dependence of output intensity on several fields, and consequently several local field factors. On the other hand, new nonlinear phenomena specifically *mediated* by local field corrections were not reported, although dramatic nonlinearities originating from dynamic local field modifications were predicted to occur in dense collections of radiating atoms driven by resonant electromagnetic fields [6]. It was shown theoretically for example, by incorporation of the local field correction in the Maxwell-Bloch equations for two-level systems subject to resonant light, that intrinsic switching of optical emission could take place. Recently, these predictions were confirmed by the observation of intrinsically bistable emission of rare earth impurities at low temperature in the compounds $Cs_3Y_2Br_9 : 10\%Yb^{3+}$, $Cs_3Lu_2Br_9 : 10\%Yb^{3+}$, and $CsCdBr_3 : 1\%Yb^{3+}$ [7–9]. Nonlinearities mediated by local field effects have also been reported in composite dielectrics [10].

In the present work, we have extended observations of intrinsic switching to a new rare earth system, namely a laser glass doped with Yb and Tm ions in which behavior that is qualitatively different from earlier observations is found. Bistable emission is reported at room temperature and multistability is observed for the first time to our knowledge. The influence of the intrinsic switching process on the stimulated emission from a channel waveguide fabricated in this material is also investigated and found to be strikingly different from conventional devices. We show that in this glass system optical switching involves an interplay in dynamics of two sensitizers Yb and Tm. We consider whether multistable emission arises from the same local field mechanism identified in earlier work [7], or whether

it necessitates a new nonlinear mechanism. Our experimental results are immediately relevant to a variety of compact laser systems utilizing concentrated Yb-doped gain media in which reliable, reproducible energy storage or constant output intensities are desired, such as Er, Yb-fiber amplifiers for communications [11] and table-top terawatt laser systems. However we also believe they are pertinent to laser materials utilizing high concentrations of many other rare earth ions.

We examined the optical properties of glass specimens prepared by Corning. The batch melts consisted of 12.50% Na_2O, 3.53% K_2O, 4.08% BaO, 73.70% SiO_2, and 5.99% Yb_3O_2 by weight. In addition, the starting material for the rare earth component contained 38 parts per million Tm_2O_3. The final composition thus included Yb^{3+} and Tm^{3+} ions in a concentration ratio of nearly 30,000 to 1. Other rare earth oxides, including Er_2O_3 and Ho_2O_3, were present in such low concentrations (less than 10 parts per million) as not to influence our measurements. Bulk samples were cut from the optical grade glass specimen into 1x10x10 mm^3 slabs and polished to a mirror finish. Additionally, in one sample, waveguides were prepared by etching parallel strips 10 μm wide through an aluminum mask evaporated onto one surface of the glass slab. Silver was then diffused into the exposed glass surface by immersion in a sodium nitrate–silver nitrate (0.5% $AgNO_3$ by weight) melt for 12 minutes. This created silver rich channels 10 μm wide and up to 5 μm deep in which the refractive index differed by 0.03 from that of the surrounding glass [12].

In all, seven channels with transmission losses less than 3 dB at 1020 nm were formed in the waveguide sample. Laser cavities were subsequently formed by placing a pair of plane dichroic mirrors perpendicular to the channel ends. Index matching fluid was used to minimize coupling losses. The mirrors had a transmission of 80% at 910 nm and a reflectance of 95% at 1020 nm. To observe bistability in bulk samples, we monitored the intensity of Tm^{3+} and Yb^{3+} emissions at 483 nm and 960 nm respectively, while varying the power of the exciting beam. For waveguide measurements, the intensity of these emissions was monitored perpendicular to the channels, together with the laser output power at 1020 nm in the forward direction. Luminescence was split into two portions with a mirror and simul-

taneously analyzed at 483 and 960 nm with a pair of Czerny-Turner spectrometers equipped with photon-counting electronics.

A continuous-wave Ti:Sapphire laser was used as the exciting source. Its output power was stabilized and controlled with an electro-optic servo. Bulk samples were excited at a wavelength of 973 nm, corresponding to the strongest absorption peak of the Yb^{3+} ion in this glass host. In the case of the waveguide laser however, the transmission of the high reflector was too low and the absorption in the channel too high at 973 nm to provide reasonable gain over the whole length of the waveguide channel. Hence the guide was instead pumped at 910 nm, a wavelength corresponding to a secondary absorption peak of Yb^{3+} (Fig. 1 inset). This provided reasonable pumping efficiency without any change of output coupling. Near-infrared measurements of laser output power were made with a pyroelectric detector.

Portions of the emission spectrum excited at room temperature by absorption on the $^2F_{5/2} \rightarrow {}^2F_{7/2}$ transition of Yb^{3+} at 970 nm are shown in Fig. 1. Identical spectra were observed in the bulk and waveguide samples. The main figure shows lines in the blue centered at 483 nm and attributed to $^1G_4 \rightarrow {}^3H_6$ emission of the Tm^{3+} ion, together with a red band near 650 nm assigned to $^3F_3 \rightarrow {}^3H_6$ transitions in the same ion. In the inset is the near-infrared emission spectrum from the $^2F_{5/2}$ state of Yb^{3+} in this sample, with an anomalous feature at 910 nm whose origin is not presently understood. Both visible and near-infrared spectra have been normalized to the most intense feature in the corresponding wavelength range. The broad near-infrared band is much stronger than the visible bands. No known Tm^{3+} transitions involving single ions in the ground state occur in the wavelength range of Yb^{3+} absorption, and off-resonant single ion excitation mechanisms involving photons in this energy range have not been reported for Tm^{3+}. Nevertheless, energy transfer from Yb^{3+} to Tm^{3+} evidently does populate the excited states of Tm^{3+} [13–15], as indicated by the visible emission trace in Fig. 1. Although the concentration of Tm^{3+} is quite low, and the transfer is off-resonant, transfer efficiency is high enough [13] to ensure significant excited state populations of Tm^{3+}. Unfortunately, the configuration of centers at which Yb^{3+} ions in this material interact with Tm^{3+} and the mechanism of their interaction is unknown.

Figure 2(a) shows the observed intensities of 483 nm and 960 nm emission in the bulk sample as a function of incident power at 973 nm. The upper trace shows that the visible emission intensity drops abruptly at 370 mW, as the incident power is increased. Later, as power is lowered, it undergoes an abrupt increase at 330 mW. A distinct hysteresis loop is thereby produced. The lower trace shows corresponding behavior in the near-infrared. There too, emission intensity changes discontinuously at optical powers where the visible emission at 483 nm undergoes its sudden variations, but the sense of the hysteresis is opposite: the near-infrared emission intensity switches down when the visible switches up and vice versa. This is similar to earlier observations of intrinsic switching in other materials [7]. However, unlike previously published observations in bulk heavy metal halide crystals, the pump intensities at which switching occurred varied greatly between runs, and in some cases no switching was observed at all. This perplexing variability was virtually eliminated by moving to the waveguide geometry described next.

Results with greatly improved reproducibility were obtained in channel waveguides formed in the same glass. In Fig. 2(b), emission from a waveguide lacking end mirrors is shown. Two hysteresis loops can be discerned in traces of emission at wavelengths of 483 nm and 960 nm in the channel. The switching points at the two wavelengths occur at somewhat different input intensities, as might be expected, since visible and infrared luminescence were imaged from different points in the channel. Light originating predominantly from the exit of the channel was analyzed in the visible spectral region, whereas light from the entrance was analyzed in the infrared. The relative displacement of hysteresis loops at the two wavelengths was attributed to propagation effects, since it disappeared when laser action rendered internal fields more uniform, as we show next.

Figure 3(a) shows the variation of the intensities of visible and near-infrared emission perpendicular to the guide when the cavity is aligned for laser operation. Oscillation does not occur at 483 nm and 960 nm in the range shown, but the fluorescence intensities at these wavelengths nevertheless saturate in unison above the laser threshold, confirming the presence of significant Tm-Yb coupling. Near threshold, the near-infrared and visible emission

traces reveal switching behavior similar to that in the bulk sample (Fig. 2(a)), producing near-infrared and visible hysteresis loops with opposite sense as before. At higher power, a second hysteretic region is encountered where switching points are better aligned at the two wavelengths than in Fig. 2(b), and higher contrast is achieved. Here, curiously, the visible and near-infrared intensities switch in the same direction. Laser output at 1020 nm also exhibits saturation and switching behavior, as shown in Fig. 3(b). The laser output switching "polarities" follow the near-infrared luminescence hysteresis (Fig. 3(a)). The onset of switching is closely followed by strong saturation of the laser output power not far above threshold.

Previous theoretical analysis by several groups [7,16] identified the Lorentz local field correction as the factor responsible for polarization-population coupling which leads to bistable luminescence. Pair interactions were shown to be capable of amplifying the hysteresis [7], and recent site selective spectroscopy of intrinsic bistability in $CsCdBr_3 : Yb^{3+}$ has provided information on the roles of energy migration and ion-ion distances needed to observe intrinsic switching [8]. As presently formulated however, the local field model predicts only a cubic dependence of incident light intensity on excited state populations, and hence only a single intensity region where bistability can occur, in contrast to the data shown in several of the foregoing figures. Consequently, questions regarding the origin of multistable luminescence in the present system are immediately raised, and an explanation for observations of this phenomenon at high temperature is needed.

While we do not propose a detailed mechanism of intrinsic multistability here, it is possible to provide some perspective on why results in the waveguide were more consistent than in the bulk glass. Yb ions can interact with Tm ions either by sequential energy transfer from several excited Yb^{3+} ions to a single nearby Tm^{3+} ion [14], or a three-center process in which two excited, nearest-neighbor Yb^{3+} ions cooperatively transfer energy to a Tm^{3+} ion [15]. Whatever the excitation mechanism is, it depends on many factors: inter-ion distances, the relative concentrations of the ions, and the number of ions participating [17,18]. Hence interaction rates will vary greatly from point to point in real materials for processes involving two

or more ions. Although ion distributions in glass are often assumed to be spatially homogeneous, the local densities for specific three-ion clusters of trivalent rare earths for example, in a predominantly divalent and monovalent host environment, will vary considerably due to variations in processing conditions during manufacture, local charge compensation, and so forth. Ion clusters favorable for generating the nonlinear effects reported here is therefore expected to be irregular. Critical fluctuations in the distribution of impurity centers in this glass, together with non-uniformity of fields in absorptive materials, probably account for the extreme sensitivity to spot size and positioning of the excitation volume that we observed within bulk samples, and the subsequent improvement in reproducibility observed within waveguide channels.

The results presented here in which the relative polarities of visible and near-infrared hysteresis loops are *opposite* are consistent with the detailed balance argument of Hehlen *et al* [8]. There it was presumed that upconversion and infrared luminescent processes drew on two coupled but physically distinct groups of ions. One group accounted for visible upconversion, the other emitted primarily infrared radiation, and fast migration of energy between these groups ensured that excited ions undergoing one process were unavailable for the other. In the present experiments we find examples not only of opposite polarities of visible and near-infrared switching, but also of identical polarities in a single sample. Where identical switching polarity is observed, a single excited state population must be responsible for both the visible and the near-infrared emission. Consequently, the observation of both kinds of switching behavior in our samples presents a second challenge in modeling the switching dynamics.

In summary, we have demonstrated intrinsic switching and multistability of photoluminescence in glass doped with Yb^{3+} and Tm^{3+} impurities at room temperature. Laser emission in waveguide channels fabricated in this glass underwent hysteretic switching just above threshold at room temperature. The clamping of output power and its intrinsic instabilities seriously limited the extraction efficiency and predictability of waveguide laser output. The Lorentz local field model does not account in its present form for new features

of luminescence instabilities observed in this glass host, namely multistability and reversal of relative switching polarity of near-infrared and visible hysteresis in a single sample. Additional theoretical work is needed. Since energy transfer mechanisms similar to those described here for Yb-Tm apply also to the dynamics of Yb-Er systems, the present results can be expected to extend to Er systems and other concentrated rare earth media, introducing a new intrinsic limit to doping (and therefore compactness) of solid state oscillators and amplifiers.

REFERENCES

[1] H. A. Lorentz, *The Theory of Electrons and its applications to the phenomena of light and radiant heat* (Dover, New York, 1953), Sections 117–136 and note 54.

[2] J. Van Kranendonk and J. E. Sipe, in *Progress in Optics XV*, edited by E. Wolf (North-Holland, Amsterdam, 1977), p. 245.

[3] F. Hynne and R. K. Bullough, Philos. Trans. R. Soc. London, Ser. A **312**, 251 (1984); **321**, 305 (1987); **330**, 253 (1990).

[4] See for example, Y. R. Shen, *Principles of Nonlinear Optics* (Wiley Interscience, New York, 1984).

[5] A. Wokaun, Mol. Phys. **56**, 1 (1985).

[6] C. M. Bowden and C. C. Sung, Phys. Rev. A **19**, 2392 (1979); M. O. Scully, Phys. Rev. Lett. **67**, 1855 (1991).

[7] M. P. Hehlen, H. U. Güdel, Q. Shu, J. Rai, S. Rai, and S. C. Rand, Phys. Rev. Lett. **73**, 1103 (1994); S. R. Lüthi, M. P. Hehlen, T. Riedener, and H. U. Güdel, J. Lumin. **76** & **77**, 447 (1998).

[8] M. P. Hehlen, H. U. Güdel, Q. Shu, and S. C. Rand, J. Chem. Phys. **104**, 1232 (1996).

[9] M. Hehlen, A. Kuditcher, and S. C. Rand, Phys. Rev. Lett. (to be published).

[10] J. E. Sipe and R. W. Boyd, Phys. Rev. A . **46**, 1614 (1992); R. J. Gehr, G. L. Fischer, R. W. Boyd, and J. E. Sipe, Phys. Rev. A **53**, 2792 (1996).

[11] E. Desurvire, *Erbium Doped Fiber Amplifiers: Principles and Applications*, (Wiley Interscience, New York, 1994).

[12] R. V. Ramaswamy and S. I. Najafi, IEEE J. Quantum Electron. **QE-22**, 883, 1986.

[13] B. Peng and T. Izutami, Optical Materials **4**, 797 (1995); F. Auzel, C. R. Sci., Ser. B

263, 819 (1966).

[14] G. Huber, E. Heumann, T. Sandrock, and K. Petermann, J. Lumin. **72** & **73**, 1 (1997).

[15] V. V. Ovsyankin and P. P. Feofilov, Sov. Phys.-JETP Lett. **3**, 322 (1966).

[16] C. M. Bowden and J. P. Dowling, Phys. Rev. A **47**, 1247 (1993).

[17] D. L. Dexter, J. Chem. Phys. **21**, 836 (1953).

[18] B. Peng and T. Izutami, Optical Materials **4**, 701 (1995).

FIGURES

FIG. 1. Emission spectra of Yb^{3+} and Tm^{3+} ions in glass excited at 960 nm. The main figure shows visible emission features. The inset shows near-infrared emission. Vertical axes have been normalized to the most intense spectral peak.

FIG. 2. (a) Power dependence of visible and near-infrared luminescence intensity in a thin sample of Yb^{3+} and Tm^{3+} doped glass at room temperature. The arrows indicate the directions in which the intensities are changing. (b) Emission intensities from first half (near-infrared) and second half (visible) of a channel waveguide at room temperature versus incident power.

FIG. 3. (a) Intensity of visible and near-infrared spontaneous emission in waveguide laser cavity as the incident laser power is first increased and then decreased. Arrows show the directions of traversal of the hysteresis loops.The visible and near-infrared emissions switch with opposite polarity at the transition points in the low power region where switching occurs, while at higher intensity they switch with like polarity. The vertical arrow indicates the lasing threshold at 1020 nm. (b) Output power of the waveguide laser at 1020 nm versus incident laser power, first as it was increased and then as it was decreased. Inset: an expanded view of the high power region.

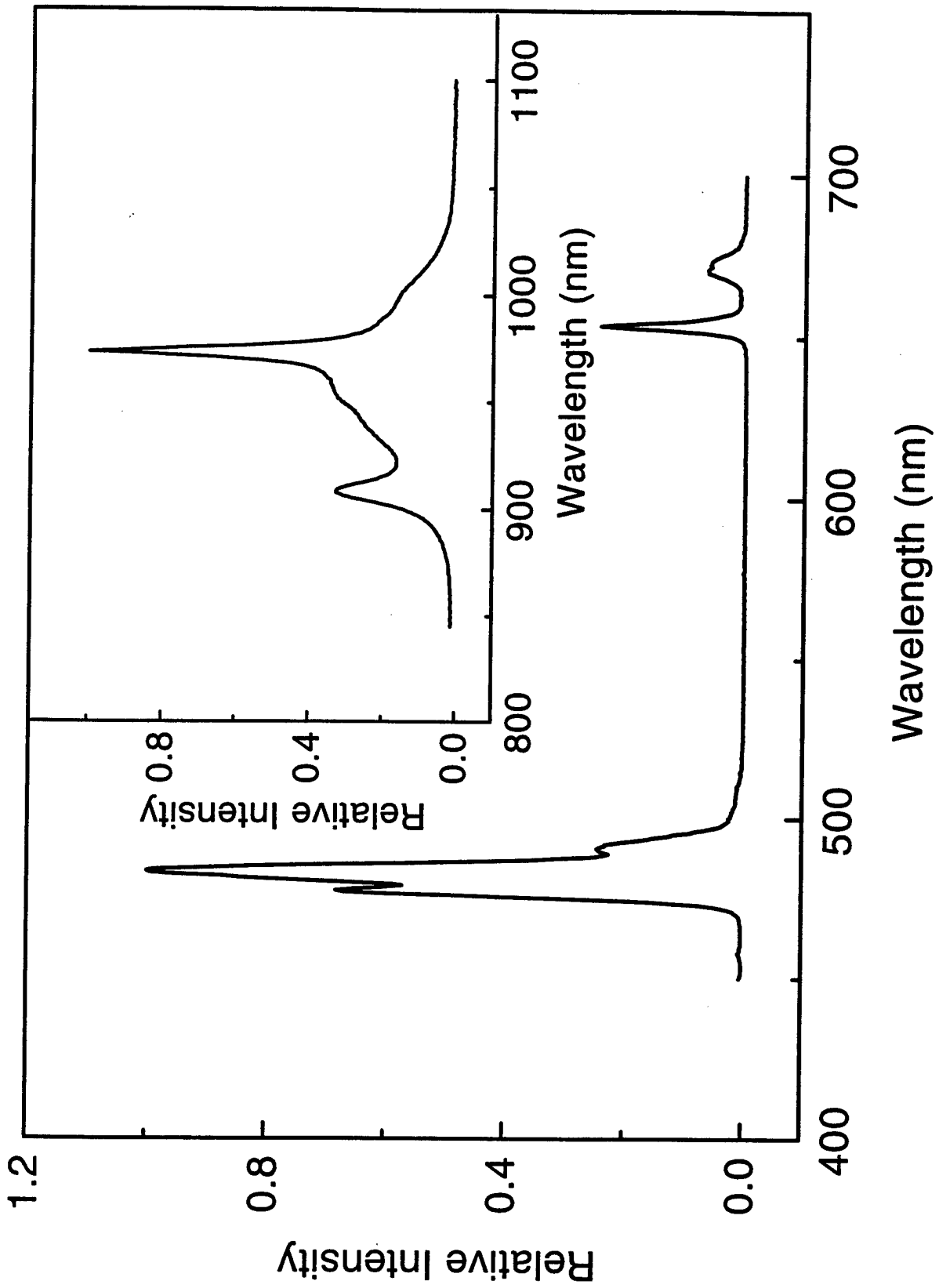
Relative Intensity
1.2
0.8
0.4
0.0
400
500
600
700
Wavelength (nm)
Relative Intensity
0.8
0.4
0.0
800
900
1000
1100
Wavelength (nm)

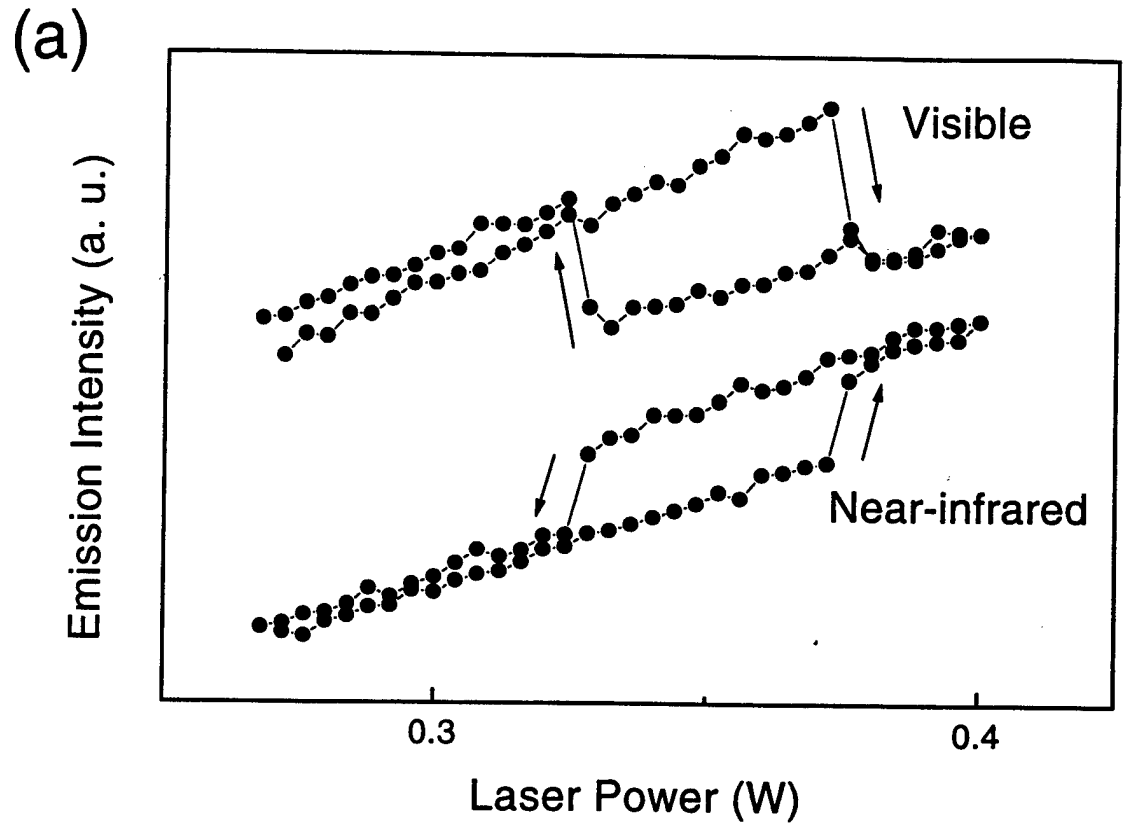
(a)
Emission Intensity (a. u.)
Visible
Near-infrared
0.3
0.4
Laser Power (W)

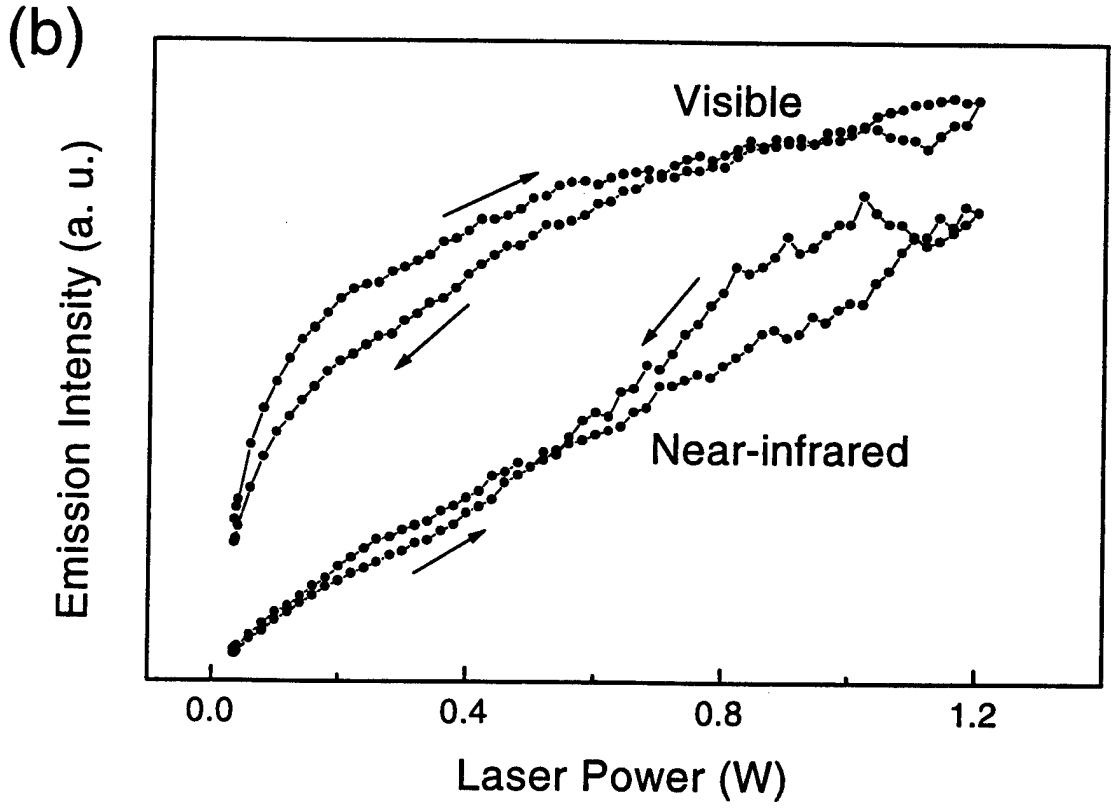
(b)
Emission Intensity (a. u.)
Visible
Near-infrared
0.0
0.4
0.8
1.2
Laser Power (W)

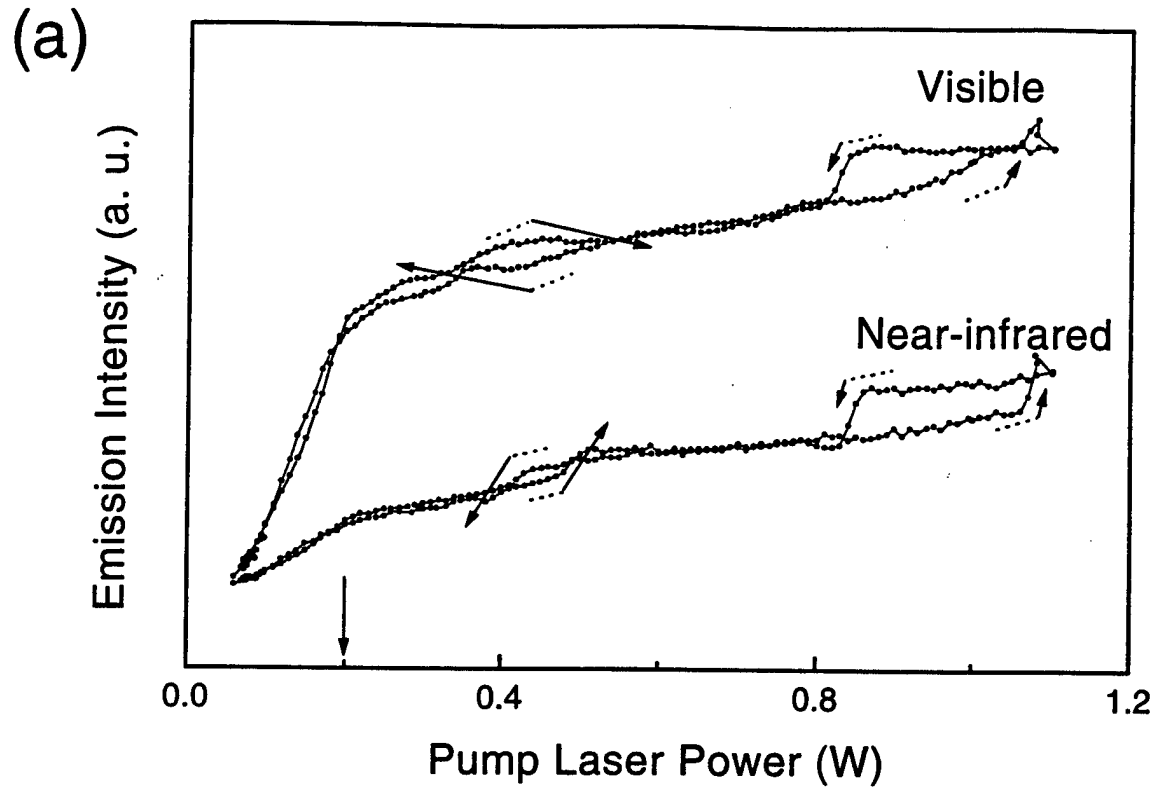
(a)
Visible
Near-infrared
Emission Intensity (a. u.)
0.0
0.4
0.8
1.2
Pump Laser Power (W)

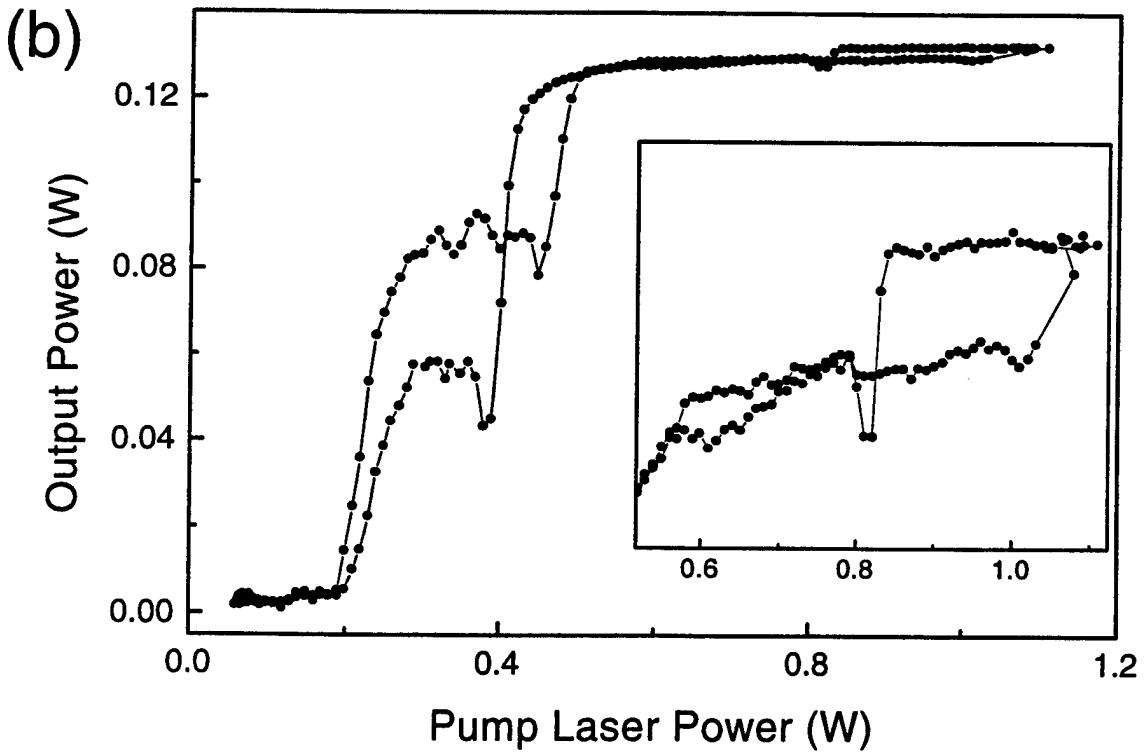
(b)
0.12
0.08
0.04
0.00
Output Power (W)
0.6
0.8
1.0
0.0
0.4
0.8
1.2
Pump Laser Power (W)

Laser action in strongly scattering rare-earth-doped dielectric nanophosphors

G. Williams, and S.C. Rand
Division of Applied Physics, Randall Laboratory
University of Michigan, Ann Arbor, MI 48109-1022
and
T. Hinklin and R.M. Laine
Dept. of Materials Science & Engineering
University of Michigan, Ann Arbor, MI 48109

ABSTRACT

We report continuous-wave "random" laser action in the ultraviolet and visible spectral regions at room temperature in δ- and of β"- alumina nanopowders doped with Ce^{3+} and Pr^{3+} respectively. To our knowledge these are the first observations of stimulated emission from electrically-pumped phosphors with scattering lengths and (virtual) cavity dimensions shorter than a wavelength, in the strong localization regime.

Evidence of quantum size effects in the luminescence of small dielectric particles [1], experiments [2-12] and theory [13-14] on localization of light and stimulated emission [15-19] in scattering media, as well as interest in the consequences of recurrent scattering events [20-21], have all heightened current interest in electromagnetic phenomena in multiple-scattering media. Traditionally, multiple scattering has been of interest to researchers studying statistical aspects of weakly localized light [22], coherence properties [23] or imaging through inhomogeneous media [24]. Others have demonstrated powder lasers in the diffusive propagation regime [4,7,11]. However, at the boundary between the diffusive and strong scattering regimes significant changes occur in the interaction of light with matter which are fundamentally new. In particular, severe scattering is predicted to cause Anderson localization of light [13-14] when absorption is negligible. Strong localization results in three-dimensional confinement of light within regions of sub-wavelength dimensions that has profound implications for the spectral bandwidth of elastically-scattered light, the visibility of the back-scattering cone, and spatial or temporal coherence of the radiation. Constitutive parameters like the dielectric constant become difficult to define [25] when propagation is restricted to sub-wavelength "transport" distances $l^* < \lambda$ in *random* media, because fluctuations in the structure of the medium and non-uniformities in the field amplitude occur on the same distance scale. Furthermore, as particles are made smaller, their surface-to-volume ratio increases and a unique class of quantum size effects can be expected to emerge in the relaxation of rare earth dopants in nanodielectrics, due to the appearance of surface-mode decay channels. Finally, the onset of recurrent (closed loop) scattering events has been predicted to reduce the threshold for laser action mediated by scattering feedback [16,19].

Here we report for the first time to our knowledge results related to this latter prediction by demonstrating continuous-wave "random" laser sources in rare-earth-doped dielectric media. We have generated ultraviolet and visible laser radiation in the strong scattering regime in dry nano-powders excited by a low current, low voltage electron beam. Earlier reports of pulsed laser action in powders were all optically-pumped experiments in rare earth material in the diffusive regime [4,7,11] or in semiconductor powders exhibiting frequency selectivity within the transition bandwidth [26]. Ref. 26 is particularly

interesting in comparison with our results. In that work, mean free transport lengths under zero gain conditions were found to be comparable to the wavelength, and recurrent scattering on closed trajectories generated laser modes at very high gain. The observation of laser modes within the transition bandwidth and angular variation of the mode distribution ruled out the possibility however that the recurrent scattering paths responsible for lasing were from regions smaller than half a wavelength in size, as required to randomize statistical properties of the stimulated emission. When recurrent scattering provides feedback for lasing from source volumes less than $(\lambda/2)^3$, the constructive and destructive interference of light required to produce mode selectivity cannot occur. For effective laser source volumes smaller than this, consistent with the requirements for strong localization, the stimulated emission spectrum should occupy the full gain bandwidth, be independent of viewing angle and exhibit no speckle. In the work on laser phosphors described here, we have observed all these unusual features, together with conventional indicators of laser action such as sharp thresholds and gain-narrowing.

Particles of δ- (or β"-) alumina were synthesized by flame spray pyrolysis of organic precursors, and a dopant level of 1000±100 ppm Ce^{3+} (or Pr^{3+}) ions was easily achieved. We used an alumatrane ($N(CH_2CH_2O)_3Al$) precursor, consisting of alumatrane, 2 wt% Al_2O_3 and 0.003% CeO_2 or PrO_2 in ethanol, and produced powders by combustion [27] at a rate of 50 g/hr. Particle sizes and concentrations were estimated using BET [28] surface areas (79.5±1 and 43.2±0.2 m^2/g for Ce and Pr) and x-ray line-broadening. The unaggregated, single crystal nature of the particles was confirmed by transmission electron microscopy. The size distribution was broad, but accurately Gaussian and the dopant concentration corresponded to 75 dopant ions per 20 nm particle in the case of Ce-doping and 800 dopant ions per 40 nm particle for Pr.

As-grown powders were excited at low current and voltage with an electron beam to record optical emission spectra, and coherent back-scattering experiments at several different wavelengths [6, 29-32] were performed to measure $l^*(\lambda)$, the mean distance over which fields propagate before becoming directionally-randomized. Highly-scattering powders are normally difficult to pump and study optically because the very

scattering which provides feedback for laser action causes pump light to be scattered backwards very efficiently as it enters the medium. Incident light does not penetrate the medium well and the overall efficiency of pumping and lasing processes is destined to be low. Consequently, we chose electron excitation for our emission studies rather than the high-energy, optical pulses used in previous work. Loose powder samples were lightly pressed into a shallow, disk-shaped recess machined into an oxygen-free copper holder and placed in an ultrahigh vacuum chamber operated at a pressure of $7x10^{-10}$ Torr. A steerable beam of electrons with energies in the 1-10 keV range was lightly focused to spot diameters in the range ϕ = 2-7 mm on the sample. Luminescence was analyzed through a MgF_2 optical port with a 1 meter Czerny-Turner spectrometer.

Emission spectra recorded at various electron currents in Ce:Al_2O_3 powder (Fig. 1) showed no dependence on observation angle with respect to the sample surface normal, and no changes were observed in optical spectra of samples held in vacuum or air for up to six months. A broad feature due to the 5d-4f inter-configurational transition of Ce^{3+} [33] dominates the spectrum near 28,000 cm^{-1} at high currents. A small shoulder on the low-energy side of the main peak near 25,500 cm^{-1} disappears once the current exceeds 12 μA. Its separation from the feature at 28,000 cm^{-1} is consistent with the $^2F_{5/2}$ - $^2F_{7/2}$ interval (~2,100 cm^{-1}) of the spin-orbit split ground term observed in fluoride single crystals [34,35]. Its disappearance above 12 μA is indicative of quenching, as expected at the onset of stimulated emission on the 5d-4f($^2F_{5/2}$) transition originating from the same upper state as the 5d-4f($^2F_{7/2}$) transition. The shift of the main peak to shorter wavelengths as current increases is also consistent with the inference of gain on the 5d-4f($^2F_{5/2}$) transition, since increasing gain progressively offsets losses from resonant re-absorption.

In Fig. 2, the integrated intensity of Ce^{3+} emission is plotted versus electron current. A sharp break in the observed slope is evident at a current of ~12 μA, and narrowing of the experimental linewidth (inset) sets in abruptly at the same current. The sigmoidal variation of linewidth with current is uniquely characteristic of laser action with feedback, as opposed to amplified spontaneous emission (ASE) [36]. Since the small particle sizes in our samples preclude optical feedback from high-Q morphological

resonances either between or within powder grains, a virtual cavity mechanism is necessary to account for this [37].

Scattering conditions in the powder samples were evaluated using a standard rotating sample approach to coherent back-scattering (CBS) [6, 30]. The sample was rotated axially about the surface normal at 1 rpm, while a second stepper-motor-controlled rotation stage provided angular scanning in the horizontal plane with respect to the incident beam. A polarization analyzer, detection aperture, wavelength filter, and photomultiplier were mounted behind the incident wave beamsplitter, in the exact back-scattering direction. Probe light from an ultraviolet Ar^+ laser was pre-filtered with a monochromator to select light at 363.8 nm, overlapping the 5d – 4f(^{4}F) fluorescence of Ce^{3+}. After collimation, the 3mm beam impinged on the sample surface and the back-scattered intensity was recorded over an angular range of ±300 mrad with a step-size of 2.8 mrad, matching the detector solid angle. For measurements on Pr-doped samples, a He-Ne laser at 632.8 nm was used. Data are shown in Fig. 3.

The observation of a broad back-scattering cone indicated that the medium was lossless on length scales comparable to the mean free transport length. Theoretically, contributions to the coherent peak are summed to infinite path length [30]. This is significant in itself, since absorptive losses would greatly reduce the likelihood of achieving net optical gain and would be inconsistent with later conclusions. Least squares fits to the data [6] yielded $l^* = 169 \pm 7$ nm at 363.8 nm, and $l^* = 314 \pm 12$ nm at 632.8 nm. These values relied on an upper limit for l* of 1.2 μm determined photographically (see below), and analysis of the initial slope of the cone which gave lower limits for the internal reflectivities at 364 nm and 633 nm of $R \geq 0.981$ and $R \geq 0.984$ respectively. Mean free transport distances were therefore less than half a wavelength in both cases and the wavelength dependence of l* was weak. Our finding of near-unity reflectivities is consistent with evanescent waves whose total internal reflection can be partially frustrated by proximity of the electron deposition region to the powder surface.

Several other observations indicated strong scattering in our powders. As stated earlier, when the transport mean free path is shorter than the spatial scale necessary for interference, namely half a wavelength, stimulated *emission* should be free of speckle. Indeed, none was observed by eye in purple Ce emission or in red emission from Pr powders. Scattering of a He-Ne beam produced speckle on an angular scale determined by the beam diameter, but speckle was absent in angle-resolved CCD images of *emission* for solid angles from $6x10^{-4}$-$1.6x10^{-10}$ sr. This ruled out lateral coherence lengths greater than 2 μm, independently of CBS measurements. Back-scattering traces obtained with sample rotation about the surface normal were the same as from stationary samples for detector apertures larger than the beam diameter. Hence intensity fluctuations from source coherence were entirely absent in our samples [38]. Also, the ratio of coherent peak intensity to incoherent background was consistently 1.41/1, much less than the 2/1 contrast expected theoretically in the diffusive regime. This is a manifestation of recurrent scattering [20] from sub-wavelength source regions ($l^* < \lambda$).

Additional perspective is provided by results for luminescent intensity versus current in a second type of sample, namely a Pr:β"-Al_2O_3 powder excited at various electron energies. In Fig. 4, thresholds appear for emission on a Pr^{3+} transition in the red spectral region, just as for ultraviolet emission in Ce^{3+}-doped material. Changes in luminescence slopes are abrupt at low energies, moving to lower currents and becoming less distinct as the energy per incident particle increases. The upper slope of luminescent output versus current also increases steeply. The inset of Fig. 4 contains raw spectral emission data from the Pr sample, dominated by features at 15,810 cm^{-1} and 16,000 cm^{-1}. Because the separation of these features is the same as that expected between the two dominant spectroscopic sites in Pr:β"-Al_2O_3, these lines could be assigned to the $^3P_0 \rightarrow {}^3H_6$ (4964 cm^{-1} π) transition and the $^3P_0 \rightarrow {}^3H_6$ (4769 cm^{-1} σ) transition of Pr^{3+} respectively, or to one of these transitions at two different sites [39]. Because quenching is not observed on the red doublet as current is varied, we favor the latter assignment. Most other features in the blue-red spectral region arise from $^3P_0$, $^3P_1$, and $^3P_2$ emissions, transitions from $^1I_6$ and $^1D_2$ being spin-forbidden. At higher energy in the ultraviolet, three weak, broad bands are observed which are tentatively ascribed to broad $^1S_0$ lines terminating in ^3P, ^1D, and ^1G levels [40].

Several trends evident in Fig. 4 are explicable in terms of electron penetration in Al_2O_3, which we calculated as a function of electron energy using the Monte Carlo code CASINO [41]. In the range 1-3 keV, the average penetration depth at 20 μA was less than the mean transport distance l*, making it less than the length scale over which radiative transport was effective. Hence *significant radiant losses* from the excitation volume to the (non-inverted) surrounding medium were possible in this energy range. On this basis, it is understandable that the observed threshold was strongly dependent on voltage between 1-3 keV, being highest for the lowest voltage. At a *fixed current* of 20 μA, the voltage threshold for laser action was reached experimentally in the neighborhood of 4-5 keV. The calculated penetration depth at this threshold voltage was comparable to the measured value of l*. Under these conditions, energy deposition within the localization volume $(\sim l^*)^3$ should be most efficient in generating laser radiation [42], since it occurs on the minimum length scale consistent with low-loss, recurrent-scattering feedback.

The distinctive threshold behavior evident in Figs. 2(a) and 4, and the sigmoid line-narrowing dependence in Fig.2(b) furnish solid evidence of laser action (as opposed to ASE) in our samples excited in the range 1-4 keV. At higher voltages, the experimental plots developed more curvature, suggesting that amplified spontaneous emission may contribute when energy deposition becomes excessive. CBS observations indicate that scattering is so severe within our samples that $l^* < \lambda/2$, which precludes mode structure and frequency selectivity in stimulated emission altogether. Laser output is then incoherent, a characteristic uniquely attributable to evanescent waves [38]. The entire bandwidths of inverted transitions experience growth in Ce and Pr samples, and observations are independent of angle, showing that electron excitation readily generates truly "random" laser action in doped oxide nano-crystals at room temperature. Our results are the first to demonstrate continuous-wave laser action on the ultraviolet 5d-4f transition of Ce^{3+} by any means. The results for Ce and Pr together indicate broad applicability of our methodology to the generation of stimulated radiation at many wavelengths. The mild conditions found necessary to sustain stimulated emission in laser

phosphors support the idea that thresholds are lowered significantly by the recurrent scattering events accompanying strong localization [16].

Many applications for evanescent laser sources emitting incoherent light can be imagined in conventional lighting and displays, since existing phosphors in televisions, fluorescent lights, plasma and field emission displays all rely on spontaneous rather than stimulated emission. The low, fixed rate of spontaneous emission normally presents a strict limit to the achievable brightness in a given light-emitting material, but stimulated emission in principle removes this limitation. The absence of speckle from evanescent sources could facilitate large-area, sub-micron optical lithography for example. But while doped, dielectric nanophosphors can provide a versatile family of materials for novel, bright light sources, many fundamental advances will also emerge from this research. Nonlinear optics with evanescent waves in layers of these novel gain media less than a wavelength thick will be enabled, and new phenomena associated with nonlinear recurrent scattering and size effects can be anticipated. Stimulated emission will be achieveable in nanopowders on new transitions, in new wavelength ranges, with approaches to medium excitation not previously feasible in dielectrics. The study of statistical properties of light such as spatial and temporal coherence, speckle and back-scattering across the photon localization boundary will be possible. Unlike the situation in electron localization, the interaction of photons with one another is negligible at low energies and amplification and parametric processes take place in electromagnetic waves. Consequently, research on these topics should furnish uniquely interesting perspectives on particle, charge and wave transport in disordered systems of many kinds, and may even help in the elucidation of mechanisms of galaxy masers [43].

The authors deeply appreciate support from AFRL (K. Schepler) and the Air Force Office of Scientific Research (H. Schlossberg) at early stages of this research and grant DMR-9975542 from the National Science Foundation. J. Williams helped with synthesis and A. Harris assisted with scattering measurements. We acknowledge useful discussions with E. Leith and O. Stafsudd, and thank S. Lipson for interesting us in laser paints.

References

1. B.M. Tissue, Chem. Mater. 10, 2837-2845(1998).

2. M. P. Van Albada and A. Lagendijk, Phys. Rev. Lett. 55, 2692(1985).

3. M. Kaveh, M. Rosenbluh, I. Edrei, and I. Freund, Phys. Rev. Lett. 57, 2049(1986).

4. V.M. Markushev, V.F. Zolin, and Ch. M. Briskina, Sov. J. Qu. El. 16, 281(1986).

5. A.Z. Genack and N. Garcia, Phys. Rev. Lett. 66, 2064(1991).

6. J.X. Zhu, D.J. Pine, and D.A. Weitz, Phys. Rev. A44, 3948-3959 (1991).

7. C. Gouedard, D. Husson, C. Sauteret, F. Auzel, and A. Migus, J.O.S.A. B10, 2358-2363 (1993).

8. N.M. Lawandy, R.M. Balachandran, A.S.L. Gomes and E. Sauvain, Nature 368, 436-438 (1994).

9. W.L. Sha, C.-H. Liu, and R.R. Alfano, Opt. Lett. 19, 1922(1994).

10. M. Siddique, R.R. Alfano, G.A. Berger, M. Kempe, and A.Z. Genack, Opt. Lett. 21, 450(1996).

11. M.A. Noginov, N.E. Noginov, H.J. Caulfield, P. Venkateswarlu, T. Thompson, M. Mahdi, and V. Ostroumov, J.O.S.A. B13, 2024(1996).

12. D. Wiersma and A. Lagendijk, Physics World, 33-37, January 1997.

13. S. John, Phys. Rev. Lett. 53, 2169(1984).

14. P.W. Anderson, Phil. Mag. B52, 505(1985).

15. V.S. Letokhov, Sov. Phys. JETP 26, 835(1968).

16. S. John and G. Pang, Phys. Rev. A54, 3642-3652 (1996).

17. R.M. Balachandran, N. M. Lawandy, and J.A. Moon, Opt. Lett. 22, 319(1997).

18. D. Wiersma and A. Lagendijk, Phys. Rev. E54, 4256-4265 (1996).

19. G.A. Berger, M. Kempe, and A.Z. Genack, Rev. E56, 6118(1997).

20. D.S. Wiersma, M.P. van Albada, B.A. van Tiggelen, and A. Lagendijk, Phys. Rev. Lett. 74, 4193-4196 (1995).

21. D.S. Wiersma, P. Bartolini, A. Lagendijk and R. Rhigini, Nature 390, 671(1997).

22. M. Kaveh, M. Rosenbluh and I. Freund, Nature 326, 778(1987)

23. G. Gbur and E. Wolf, Opt. Lett. 24, 10(1999); E. Wolf, T. Shirai, G. Agarwal, L. Mandel, Opt. Lett. 24, 367(1999).

24. E. Leith, C. Chen, H. Chen, Y. Chen, D. Dilworth, J. Lopez, J. Rudd, P.-C. Sun, J. Valdmanis, and G. Vossler, J.O.S.A. A9, 1148(1992).

25. R.W. Boyd and J.E. Sipe, J.O.S.A. B11, 297(1994).

26. H.Cao, Y.G. Zhao, S.T. Ho, E.W. Seelig, Q.H. Wang, and R.P.H. Chang, Phys. Rev. Lett. 82, 2278(1999).

27. A.C. Sutorik, S.S. Neo, T. Hinklin, R. Baranwal, D.R. Treadwell, R. Narayanan, and R.M. Laine, J. Am. Ceram. Soc. 81, 1477-1488 (1998); R.M. Laine, K. Waldner, C. Bickmore, D. Treadwell, U.S. Patent 5,614,596 (March 1997).

28. S. Brunauer, P.H. Emmett, and E. Teller, J. Am. Chem. Soc. 60, 309(1938).

29. Y. Kuga and A. Ishimura, J.O.S.A. A1, 831(1984).

30. P.E. Wolf and G. Maret, Phys. Rev. Lett. 56, 1471(1986).

31. E. Akkermans, P.E. Wolf, R. Maynard, and G. Maret, J. Phys. (Fr) 49, 77-98 (1988).

32. E. Akkermans, P.E. Wolf, and R. Maynard, Phys. Rev. Lett. 56, 1471(1986).

33. S. Okamoto, K. Kato and T. Arakawa, J. Alloys and Compounds 192, 37(1993).

34. D.J. Ehrlich, P.F. Moulton, and R.M. Osgood, Jr., Opt. Lett. 4, 184-186 (1979).

35. C.D. Marshall, J.A. Speth, S.A. Payne, W.F. Krupke, G.J. Quarles, V. Castillo and B.H.T. Chai, J.O.S.A. B11, 2054-2065(1994); N. Sarukura, M.A. Dubinskii, Z. Liu, V.V. Semashko, A.K. Naumov, S.L. Korableva, R.Y. Abdulsabirov, K. Edamatsu, Y. Suzuki, T. Itoh, and Y. Segawa, I.E.E.E. J. Select. Topics in Qu. El. 1, 792(1995).

36. A. Yariv, Quantum Electronics, 2nd ed., J. Wiley and Sons, N.Y. (1975).

37. R.M. Balachandran and N.M. Lawandy, Opt. Lett. 20, 1271(1995).

38. J.W. Goodman, Statistical Optics, J. Wiley and Sons, N.Y., 1985, pp. 347-356.

39. Phyllis Nelson, " A triply-ionized rare earth ion in an axial crystal field: Pr^{3+} in β-alumina", Ph. D. Dissertation, University of California Los Angeles, 1995. Site-to-site splitting taken to be that reported by B. Dunn et al., J. Sol. St. Chem. 73, 235(1988) for Nd, since the A_{20} coefficient is similar.

40. L. -S. Lee, S.C. Rand, and A.L. Schawlow, Phys. Rev. B29, 6901(1984).

41. P. Hovington, D. Drouin, and R. Gauvin, Scanning 19, 1(1997).

42. G. van Soest, M. Tomita, and A. Lagendijk, Opt. Lett. 24, 306(1999).

43. A.D. Haschick and W.A. Baan, Nature 313, 144(1985); L. Staveley-Smith, D.A. Allen, J.M. Chapman, R.P. Norris, and J.B. Whiteoak, Nature 337, 625(1989).

FIGURE CAPTIONS

Figure 1. Cathodoluminescence spectra of Ce:δ-Al_2O_3 nanoparticles excited at 4 keV by various electron beam currents in a 7 mm spot-size (T=293 K).

Figure 2. Integrated emission intensity centered at λ_{em} = 362 nm versus current. The solid curves are guides to the eye. Inset: Full width at half maximum intensity of ultraviolet emission from Ce:δ-Al_2O_3 nanoparticles plotted versus current.

Figure 3. Experimental back-scattered intensity versus angle at (a) λ_{ex}=363.8 nm and (b) λ_{ex}= 632.8 nm, from Ce:δ-Al_2O_3 and Pr:β"-Al_2O_3 nanoparticles respectively. Solid curves are least squares theoretical fits (see text).

Figure 4. Peak emission intensity versus current at λ_{em} = 633 nm in Pr:β"-Al_2O_3 nanoparticles, plotted for various electron energies in the range 1-10 keV. Inset: Emission spectra of Pr:β"-Al_2O_3 showing growth of the red transition relative to other visible and ultraviolet sample emissions at 7 keV.

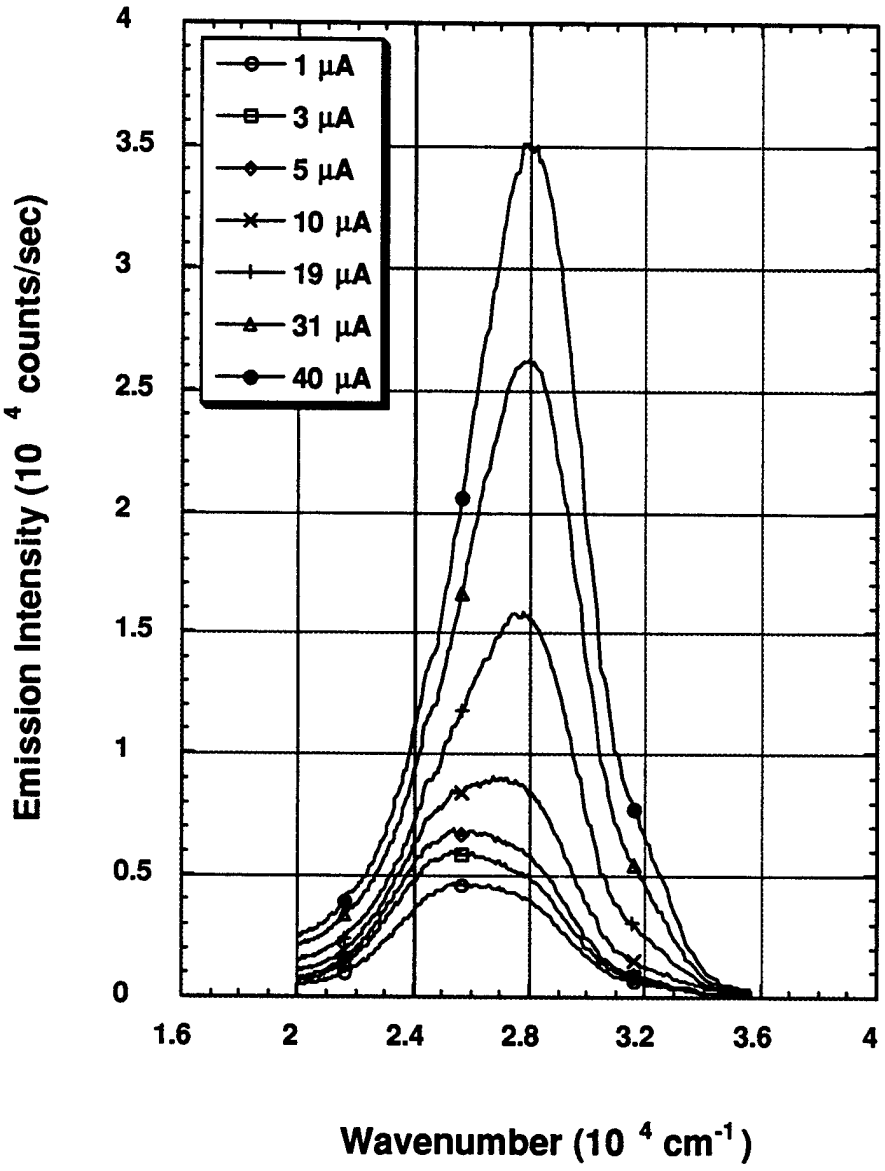
1 μA
3 μA
5 μA
10 μA
19 μA
31 μA
40 μA
Emission Intensity (10 4 counts/sec)
Wavenumber (10 4 cm-1)
0
0.5
1
1.5
2
2.5
3
3.5
4
1.6
2
2.4
2.8
3.2
3.6
4

Figure 1.

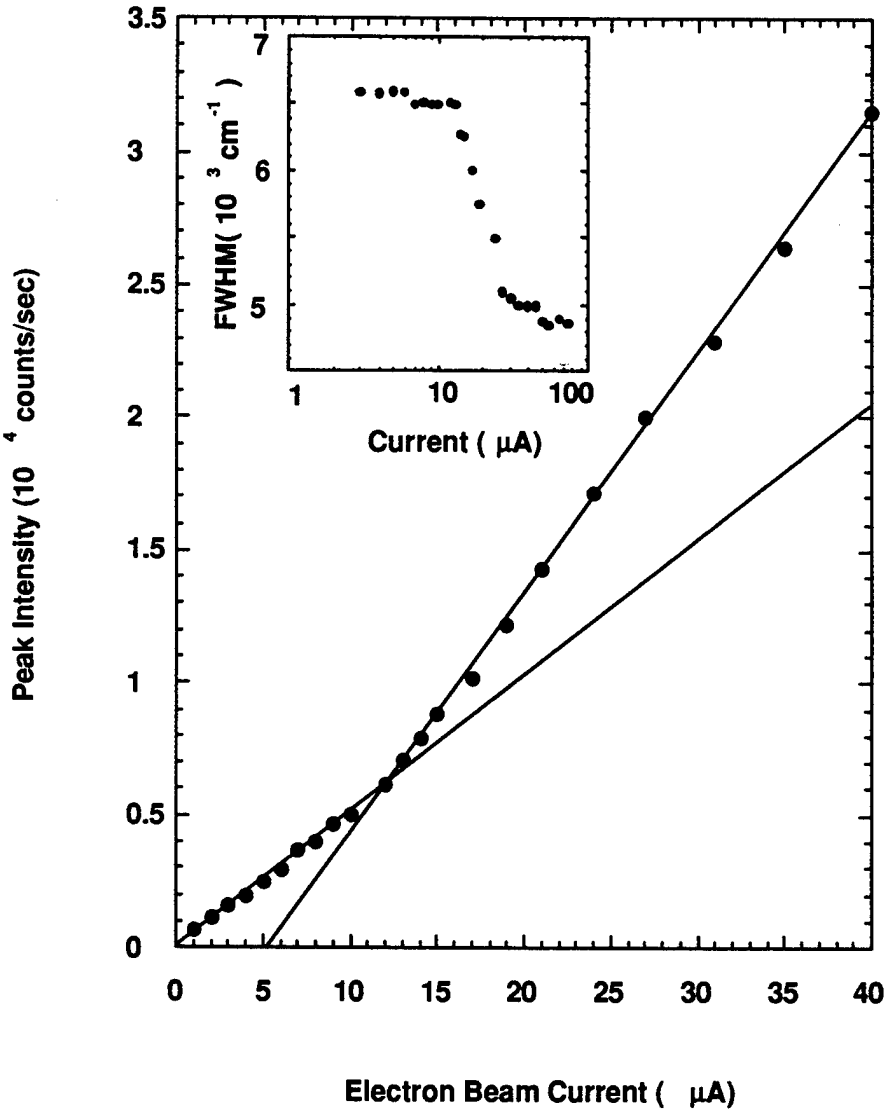
Peak Intensity (10 4 counts/sec)
3.5
3
2.5
2
1.5
1
0.5
0
0
5
10
15
20
25
30
35
40
Electron Beam Current (μA)
FWHM(10 3 cm-1)
7
6
5
1
10
100
Current (μA)

Figure 2.

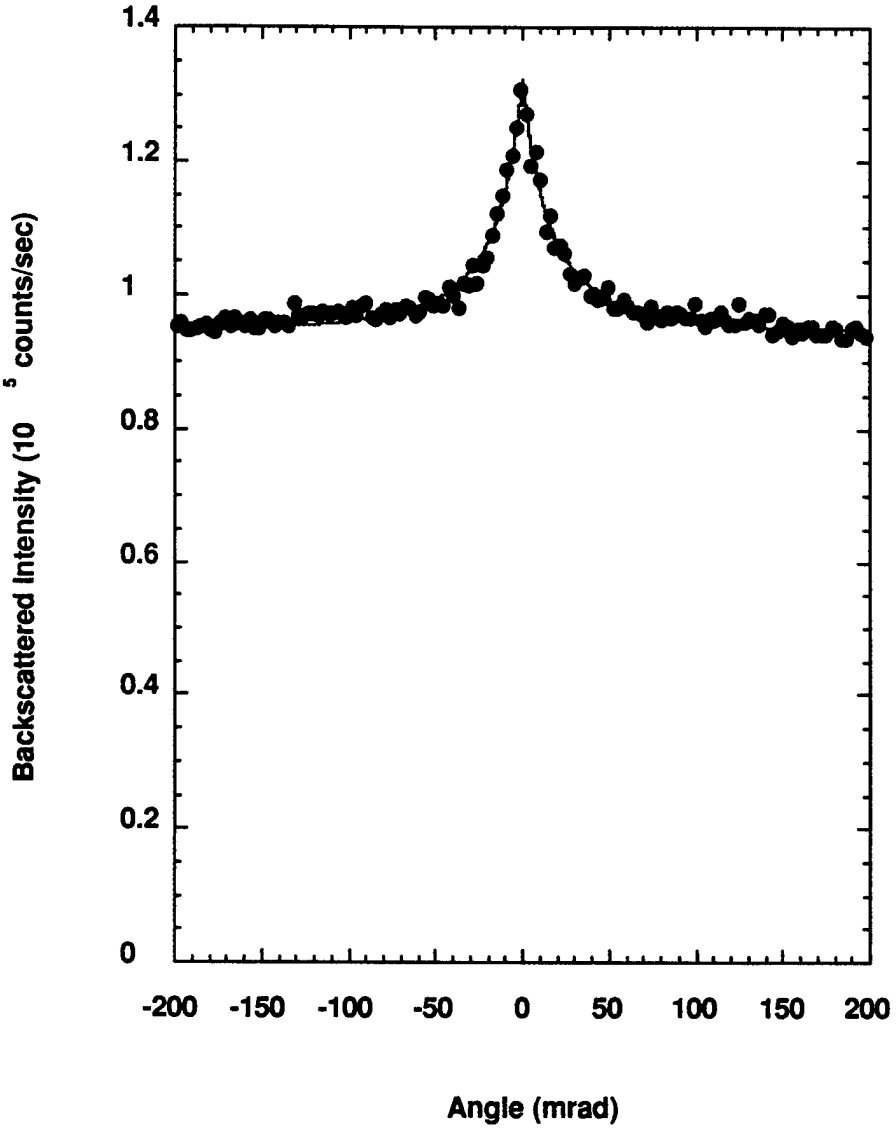
1.4
1.2
1
0.8
0.6
0.4
0.2
0
Backscattered Intensity (10 5 counts/sec)
-200
-150
-100
-50
0
50
100
150
200
Angle (mrad)

Figure 3(a)

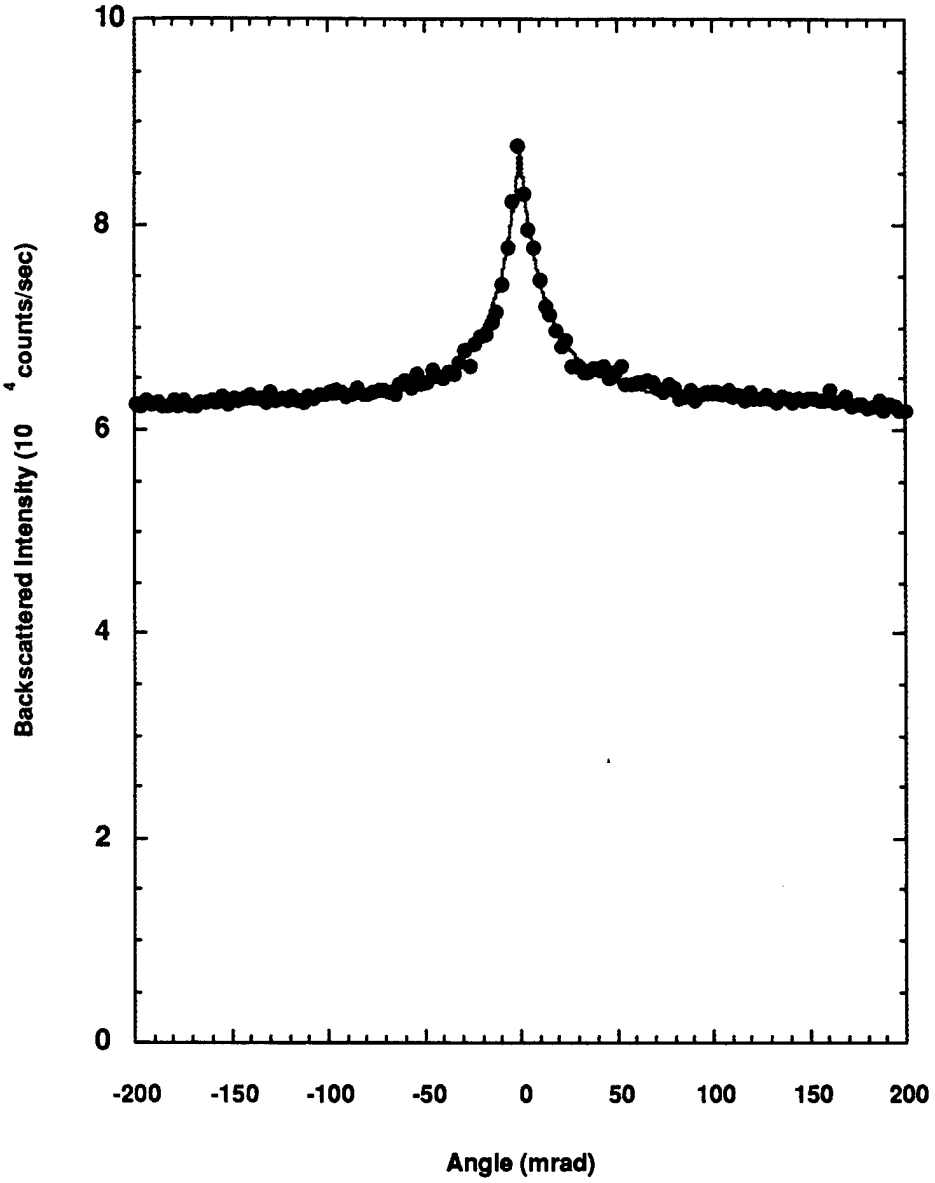
10
8
6
4
2
0
Backscattered Intensity (10 4 counts/sec)
-200
-150
-100
-50
0
50
100
150
200
Angle (mrad)

Figure 3(b).

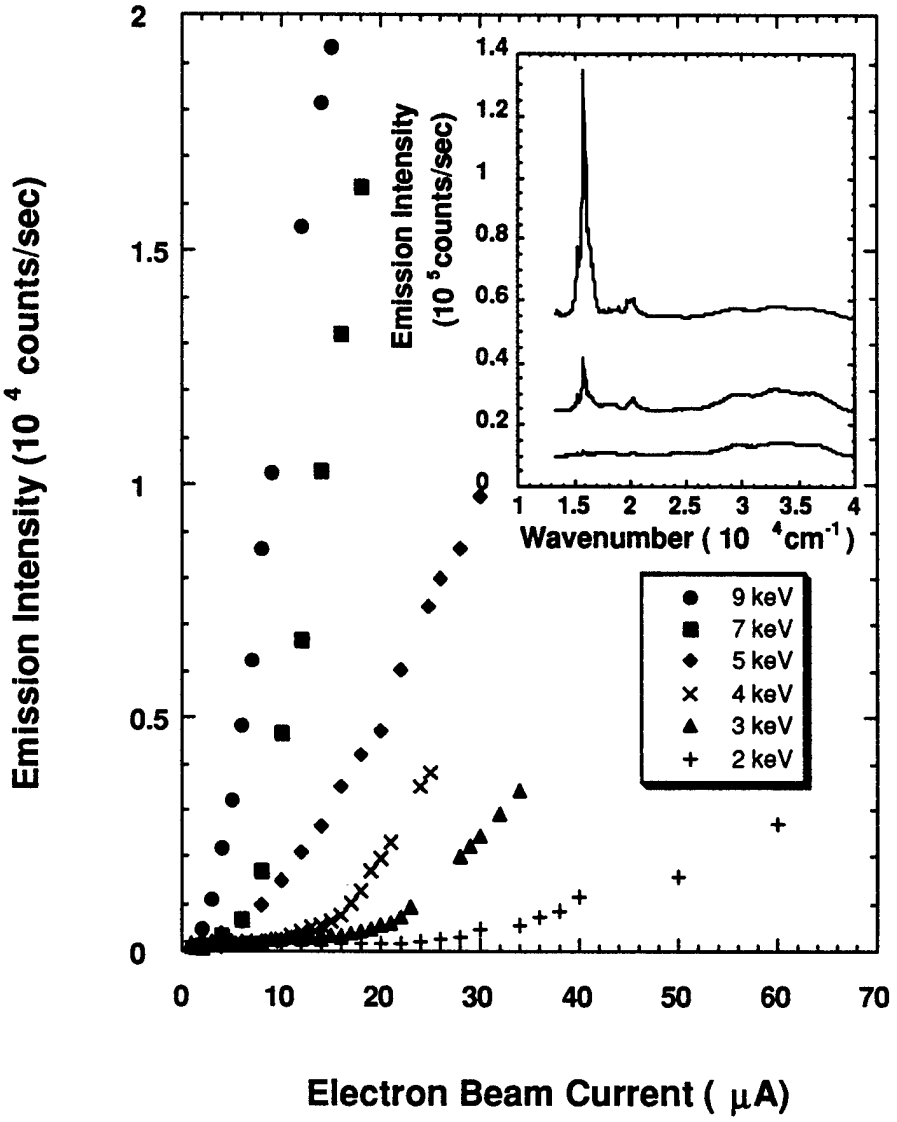
Emission Intensity (10 4 counts/sec)
Electron Beam Current (μA)
Emission Intensity (10 5 counts/sec)
Wavenumber (10 4 cm-1)
9 keV
7 keV
5 keV
4 keV
3 keV
2 keV

Figure 4.